Modelling spatial and temporal dynamics of GPP in the Sahel from earth observation based photosynthetic capacity and quantum efficiency

Torbern Tagesson[1], Jonas Ardö[2], Bernard Cappelaere[3], Laurent Kergoat[4], Abdulhakim Abdi[2], Stéphanie Horion[1], Rasmus Fensholt[1]

[1]Department of Geosciences and Natural Resource Management, University of Copenhagen, Øster Voldgade 10, DK-1350 Copenhagen, Denmark; E-Mails: torbern.tagesson@ign.ku.dk, stephanie.horion@ign.ku.dk, rf@ign.ku.dk

[2]Department of Physical Geography and Ecosystem Science, Lund University, Sölvegatan 12, SE- 223 62 Lund, Sweden, E-Mails: jonas.ardo@nateko.lu.se, hakim.abdi@gmail.com

[3]HydroSciences Montpellier, IRD, CNRS, Univ. Montpellier, Montpellier, France, E-Mail: bernard.cappelaere@um2.fr

[4]Geoscience Environnement Toulouse, (CNRS/UPS/IRD), 14 av E Belin, 31400 Toulouse, France, E-Mail: laurent.kergoat@get.obs-mip.fr

Correspondence to: Torbern Tagesson (torbern.tagesson@ign.ku.dk)

Abstract. It has been shown that vegetation growth in semi-arid regions is important for the variability of the global terrestrial CO_2 sink, which indicates the strong need for improved understanding, and spatially explicit estimates of CO_2 uptake (gross primary production (GPP)) in semi-arid ecosystems. This study has three aims: 1) to evaluate the MOD17A2H GPP (collection 6) product against eddy covariance (EC) based GPP for six sites across the Sahel; 2) to characterise relationships between spatial and temporal variability in EC based photosynthetic capacity (F_{opt}) and quantum efficiency (α) and earth observation (EO) based vegetation indices (normalized difference vegetation index (NDVI); renormalized difference vegetation index (RDVI); enhanced vegetation index (EVI); and shortwave infrared water stress index (SIWSI)); and 3) to study the applicability of EO up-scaled F_{opt} and α for GPP modelling purposes. MOD17A2H GPP (collection 6) underestimated GPP strongly, most likely because maximum light use efficiency is set too low for semi-arid ecosystems in the MODIS algorithm. Intra-annual dynamics in F_{opt} was closely related to SIWSI being sensitive to equivalent water thickness, whereas α was closely related to RDVI affected by chlorophyll abundance. Spatial and inter-annual dynamics in F_{opt} and α were closely coupled to NDVI and RDVI, respectively. Modelled GPP based on F_{opt} and α up-scaled using EO based indices reproduced in situ GPP well for all except a cropped site that was strongly impacted by anthropogenic land use. Up-scaled GPP for Sahel 2001-2014 was 736±39 g C m^{-2} y^{-1}. This study indicates the strong applicability of EO as a tool for spatially explicit estimates of GPP, F_{opt} and α; incorporating EO-based F_{opt} and α in to dynamic global vegetation models could improve global estimates of vegetation production, ecosystem processes and biogeochemical and hydrological cycles.

Keywords: Remote sensing, Gross Primary Productivity, MOD17A2H, light use efficiency, photosynthetic capacity, quantum efficiency

1 Introduction

Vegetation growth in semi-arid regions is an important sink for fossil fuel emissions. Mean carbon dioxide (CO_2) uptake by terrestrial ecosystems is dominated by highly productive lands, mainly tropical forests, whereas semi-arid regions are the main biome driving its inter-annual variability (Ahlström et al., 2015; Poulter et al., 2014). Semi-arid regions even contribute to 60% of the long term trend in the global terrestrial C sink (Ahlström et al., 2015). It is thus important to understand long-term variability of vegetation growth in semi-arid areas and their response to environmental conditions to better quantify and forecast effects of climate change.

Sahel is a semi-arid transition zone between the dry Sahara desert in the North and the humid Sudanian savanna in the South. The region has experienced numerous severe droughts during the last decades that resulted in region-wide famines in 1972-1973 and 1984–1985 and localized food shortages across the region in 1990, 2002, 2004, 2011 and 2012 (Abdi et al., 2014; United Nations, 2013). Vegetation production is thereby an important ecosystem service for livelihood in Sahel, but it is under threat. The region experiences a strong population growth, increasing the demand on ecosystem services due to cropland expansion, increased pasture stocking rates and fuelwood extraction (Abdi et al., 2014).

At the same time as we have reports of declining vegetation production, we have contradicting reports of greening of the Sahel based on earth observation (EO) data (Dardel et al., 2014; Fensholt et al., 2013). The greening of Sahel has mainly been attributed to alleviated drought stress conditions due to increased precipitation since the mid-1990s (Hickler et al., 2005). Climate is thus another important factor regulating vegetation production. Semi-arid regions, such as Sahel, are particularly vulnerable to climate fluctuations due to their dependency to moisture conditions.

Estimation of gross primary production (GPP), i.e. uptake of atmospheric CO_2 by vegetation, is still a major challenge within remote sensing of ecosystem services. Gross primary production is a main driver of ecosystem services such as climate regulation, carbon (C) sequestration, C storage, food production, or livestock grassland production. Within EO, spatial quantification of GPP generally involves light use efficiency (LUE), defined as the conversion efficiency of absorbed solar light into CO_2 uptake (Monteith, 1972, 1977). It has been shown that LUE varies in space and time due to factors such as plant functional type, drought and temperature, nutrient levels and physiological limitations of photosynthesis (Garbulsky et al., 2010; Paruelo et al., 2004; Kergoat et al., 2008). The LUE concept has been applied using various methods, either by using a biome-specific LUE constant (Ruimy et al., 1994), or by modifying a maximum LUE using meteorological variables (Running et al., 2004).

An example of an LUE based model is the standard GPP product from the Moderate Resolution Imaging Spectroradiometer (MODIS) sensor (MOD17A2). Within the model, absorbed photosynthetically active radiation (PAR) is estimated as a product of the fraction of PAR absorbed by green vegetation (FPAR from MOD15A2) multiplied with daily PAR from the meteorological data of the Global Modeling and Assimilation Office (GMAO). A set of maximum LUE parameters specified for each biome are extracted from a Biome Properties Look-Up Table (BPLUT). Then maximum LUE is modified depending on air temperature (T_{air}) and vapor pressure deficit (VPD) (Running et al., 2004). Sjöström et al. (2013) evaluated the MOD17A2 product (collection 5.1) for Africa, and showed that it underestimated GPP for semi-arid savannas in Sahel. Explanations for this underestimation were that the assigned maximum LUE from BPLUT was set too low and uncertainties in the FPAR (MOD15A2) product. Recently, a new collection of MOD17A2 at 500 m spatial resolution was released (MOD17A2H; collection 6) with an updated BPLUT, updated GMAO meteorological data, improved quality control and gap filling of the FPAR data from MOD15A2 (Running and Zhao, 2015).

It has been shown that the LUE method does not perform well in arid conditions and at agricultural sites (Turner et al., 2005). Additionally, the linearity assumed by the LUE model is usually not found as the response of GPP to incoming light follows more of an asymptotic curve (Cannell and Thornley, 1998). Investigating other methods for remotely determining GPP is thus of great importance, especially for semi-arid environments. Therefore, instead of LUE we focus on the light response function of GPP at canopy scale, and spatial and temporal variation of its two main parameters: maximum GPP under light saturation (canopy-scale photosynthetic capacity; F_{opt}), and the initial slope of the light response function (canopy-scale quantum efficiency; α) (Falge et al., 2001; Tagesson et al., 2015a). Photosynthetic capacity is a measure of the maximum rate at which the canopy can fix CO_2 during photosynthesis (μmol CO_2 m^{-2} s^{-1}) whereas α is the amount of CO_2 fixed per incoming PAR (μmol CO_2 μmol PAR^{-1}). Just to clarify the difference in LUE and α in this study; LUE (μmol CO_2 μmol $APAR^{-1}$) is the slope of a linear fit between CO_2 uptake and absorbed PAR, whereas α (μmol CO_2 μmol PAR^{-1}) is the initial slope of an asymptotic curve against incoming PAR.

It has been proven that F_{opt} and α are closely related to chlorophyll abundance due to their coupling with the electron transport rate (Ide et al., 2010). Additionally, in semi-arid ecosystems water availability is generally considered to be the main limiting factor affecting intra-annual dynamics of vegetation growth (Fensholt et al., 2013; Hickler et al., 2005; Tagesson et al., 2015b). Several remote sensing studies have established relationships between remotely sensed vegetation indices and ecosystem properties such as chlorophyll abundance and equivalent water thickness (Yoder and Pettigrew-Crosby, 1995; Fensholt and Sandholt, 2003). In this study we will analyse if EO vegetation indices can be used for up-scaling F_{opt} and α and investigate if this could offer a promising way to map GPP in semi-arid areas. This potential will be analysed by the use of detailed ground observations from six eddy covariance (EC) flux tower sites across Sahel.

The three aims of this study are:

1) To investigate if the recently released MOD17A2H GPP (collection 6) product is better at capturing GPP for Sahel than collection 5.1. We hypothesise that MOD17A2H GPP (collection 6) product will estimate GPP well for the six Sahelian EC sites, because of major changes done in comparison to collection 5.1 (Running and Zhao, 2015).
2) To characterize the relationships between spatial and temporal variability in F_{opt} and α and remotely sensed vegetation indices. We hypothesise that EO vegetation indices that are closely related to chlorophyll abundance will be most strongly coupled with spatial and inter-annual dynamics in F_{opt} and α, whereas vegetation indices closely related to equivalent water thickness will be most strongly coupled with intra-annual dynamics in F_{opt} and α across Sahel.
3) To evaluate the applicability of a GPP model based on the light response function using EO vegetation indices and incoming PAR as input data.

2 Materials and Methods

2.1 Site description

The Sahel stretches from the Atlantic Ocean in the west to the Red Sea in the east. The northern border towards Sahara and the southern border towards the humid Sudanian Savanna are defined by the 150 and 700 mm isohyets, respectively (Fig. 1) (Prince et al., 1995). Tree and shrub canopy cover is now generally low (< 5%) and dominated by species of *Balanites*, *Acacia*, *Boscia* and *Combretaceae* (Rietkerk et al., 1996). Annual grasses such as *Schoenefeldia gracilis*, *Dactyloctenium aegypticum*, *Aristida mutabilis*, and *Cenchrus biflorus* dominate the herbaceous layer, but perennial grasses such as *Andropogon gayanus*, *Cymbopogon schoenanthus* can also be found (Rietkerk et al., 1996; de Ridder et al., 1982). From the FLUXNET database (Baldocchi et al., 2001) we selected the six available measurement sites with EC based CO_2 flux data from Sahel (Table 1; Fig. 1). The sites represent a variety of ecosystems present in the region, from dry fallow bush savanna to seasonally inundated acacia forest. For a full description of the measurement sites, we refer to Tagesson et al. (2016a) and references in Table 1.

<Table 1>

<Figure 1>

2.2 Data collection

2.2.1 Eddy covariance and hydrometeorological in situ data

Eddy covariance and hydrometeorological data originating from the years between 2005 and 2013 were collected from the principal investigators of the measurement sites (Tagesson et al., 2016a). The EC sensor set-up consisted of open-path CO_2/H_2O infrared gas analysers and 3-axis sonic anemometers. Data were collected at 20 Hz rate and statistics were calculated for 30-min periods. For a full description of sensor set up and post processing of EC data, see references in Table 1. Final fluxes were filtered according to quality flags provided by FLUXNET and outliers were filtered according to Papale et al. (2006). We extracted the original net ecosystem exchange (NEE) data without any gap-filling or partitioning of NEE to GPP and ecosystem respiration. The collected hydrometeorological data were: air temperature (T_{air}; °C), rainfall (P; mm), relative air humidity (Rh; %), soil moisture at 0.1 m depth (SWC; % volumetric water content), incoming global radiation (R_g; W m^{-2}), incoming photosynthetically active radiation (PAR; μmol m^{-2} s^{-1}), VPD (hPa), peak dry weight biomass (g dry weight m^{-2}), C3/C4 species ratio, and soil conditions (nitrogen and C concentration; %). For a full description of collected data and sensor set-up, see Tagesson et al. (2016a).

2.2.2 Earth Observation data and gridded ancillary data

Composite products from MODIS/Terra covering Sahel were acquired at Reverb ECHO (NASA, 2016). Collected products were GPP (MOD17A2H; collection 6), nadir bidirectional reflectance distribution function adjusted reflectance (NBAR) (8-day composites; MCD43A4; collection 5.1) at 500*500 m^2 spatial resolution, the normalized difference vegetation index (NDVI) and the enhanced vegetation index (EVI) (16-day composites; MOD13Q1; collection 6) at 250*250 m^2 spatial resolution. The NBAR product was preferred over the reflectance product (MOD09A1), in order to avoid variability caused by varying sun and sensor viewing geometry (Huber et al., 2014; Tagesson et al., 2015c). We extracted the median of 3x3 pixels centred at the location of each EC tower. Time series of EO products were filtered according to MODIS quality control data; MOD17A2H is a gap-filled and filtered product, QC data from MCD43A2 were used for filtering of MCD43A4; and bit 2-5 (highest –decreasing quality) was used for MOD13Q1. Finally, data were gap-filled to daily values using linear interpolation.

We downloaded ERA Interim reanalysis PAR at the ground surface (W m^{-2}) with a spatial resolution of 0.25°×0.25° accumulated for each 3-hour period 2000-2015 from the European Centre for Medium-Range Weather Forecasts (ECMWF) (Dee et al., 2011; ECMWF, 2016a).

2.3 Data handling

2.3.1 Intra-annual dynamics in photosynthetic capacity and quantum efficiency

To estimate daily values of EC based F_{opt} and α, the asymptotic Mitscherlich light-response function was fitted between daytime NEE and incoming PAR using a 7-day moving window with a 1-day time step:

$$NEE = -(F_{opt}) \times (1 - e^{\left(\frac{-\alpha \times PAR}{F_{opt}}\right)}) + R_d \qquad (1)$$

where F_{opt} is CO_2 uptake at light saturation (photosynthetic capacity; μmol CO_2 m^{-2} s^{-1}), R_d is dark respiration (μmol CO_2 m^{-2} s^{-1}), and α is the initial slope of the light response curve (quantum efficiency; μmol CO_2 μmol PAR^{-1}) (Falge et al., 2001). By subtracting R_d from Eq. 1, the function was forced through zero and GPP was thereby estimated. To assure high quality of fitted parameters, parameters were excluded from the analysis when fitting was insignificant (p-value>0.05), and when they were out of range (F_{opt} and α >peak value of the rainy season times 1.2). Additionally, outliers were filtered following the method by Papale et al. (2006) using a 30-day moving window with a 1-day time step.

2.3.2 Vegetation indices

The maximum absorption in red wavelengths generally occurs at 682 nm as this is the peak absorption for chlorophyll a and b (Thenkabail et al., 2000), which makes vegetation indices that include the red band sensitive to chlorophyll abundance. By far the most common vegetation index is NDVI (Rouse et al., 1974):

$$NDVI = \frac{(\rho_{NIR} - \rho_{red})}{(\rho_{NIR} + \rho_{red})} \qquad (2)$$

where ρ_{NIR} is the reflectance factor in near infrared (NIR) band (band 2) and ρ_{red} is the reflectance factor in the red band (band 1). Near infrared radiance is reflected by leaf cells since absorption of these wavelengths would result in overheating of the plant whereas red radiance is absorbed by chlorophyll and its accessory pigments (Gates et al., 1965). Normalization is done to reduce effects of atmospheric errors, solar zenith angles, and sensor viewing geometry, as well as increasing the vegetation signal (Qi et al., 1994; Inoue et al., 2008).

A well-known deficiency of NDVI is problems of index saturation at high biomass because absorption of red light at ~670 nm peaks at higher biomass loads whereas NIR reflectance continues to increase due to multiple scattering effects (Mutanga and Skidmore, 2004; Jin and Eklundh, 2014). By reducing atmospheric and soil background influences, EVI is designed to increases the signal from the vegetation and maintain sensitivity in high biomass regions (Huete et al., 2002).

$$EVI = G\frac{(\rho_{NIR} - \rho_{red})}{(\rho_{NIR} + C_1\rho_{red} - C_2\rho_{blue} + L)} \qquad (3)$$

where ρ_{blue} is the reflectance factor in the blue band (band 3). The coefficients C_1=6 and C_2=7.5 correct for atmospheric influences, while L=1 adjust for the canopy background. The factor G=2.5 is a gain factor.

Another attempt to overcome problems of NDVI saturation was proposed by Roujean and Breon (1995) who suggested the renormalized difference vegetation index (RDVI) that combines advantages of DVI (NIR-red) and NDVI for low and high vegetation cover, respectively:

$$\mathrm{RDVI} = \frac{(\rho_{NIR} - \rho_{red})}{\sqrt{(\rho_{NIR} + \rho_{red})}} \quad (4)$$

As a non-linear index, RDVI is not only less sensitive to variations in geometrical and optical properties of unknown foliage but also less affected by solar and viewing geometry (Broge and Leblanc, 2001). RDVI was calculated based on NBAR bands 1 and 2.

The NIR and SWIR bands are affected by the same ground properties, except that SWIR bands are also strongly sensitive to equivalent water thickness. Fensholt and Sandholt (2003) proposed a vegetation index, the shortwave infrared water stress index (SIWSI), using NIR and SWIR bands to estimate drought stress for vegetation in semi-arid environments:

$$\mathrm{SIWSI}_{12} = \frac{(\rho_{\mathrm{NIR}} - \rho_{\mathrm{SWIR12}})}{(\rho_{\mathrm{NIR}} + \rho_{\mathrm{SWIR12}})} \quad (5)$$

$$\mathrm{SIWSI}_{16} = \frac{(\rho_{\mathrm{NIR}} - \rho_{\mathrm{SWIR16}})}{(\rho_{\mathrm{NIR}} + \rho_{\mathrm{SWIR16}})} \quad (6)$$

where ρ_{swir12} is NBAR band 5 (1230-1250 nm) and ρ_{swir16} is NBAR band 6 (1628-1652 nm). As the vegetation water content increases, reflectance in SWIR decreases indicating that low and high SIWSI values point to sufficient water conditions and drought stress, respectively.

2.3.3 Incoming PAR across Sahel

A modified version of the ERA Interim reanalysis PAR was used in the current study as an error in the code producing these PAR estimates was identified by the data distributor causing PAR values to be too low (ECMWF, 2016b). Accordingly, incoming PAR at the ground surface from ERA Interim was systematically underestimated even though it followed the pattern of PAR measured at the six Sahelian EC sites (Fig. S1 in supplementary material). In order to correct for this error, we fitted and applied an ordinary least square linear regression between in situ PAR and ERA Interim PAR (Fig. S1). The produced PAR from this relationship is at the same level as in situ PAR and should be at a correct level even though the original ERA Interim PAR is actually produced from the red and near infrared part of the spectrum.

2.4 Data analysis

2.4.1 Coupling temporal and spatial dynamics in photosynthetic capacity and quantum efficiency with explanatory variables

The coupling between intra-annual dynamics in F_{opt} and α and the vegetation indices for the different measurement sites were studied using Pearson correlation analysis. As part of the correlation analysis, we used bootstrap simulations with 200 iterations from which mean and standard deviation of the correlation coefficients were calculated (Richter et al., 2012). Relationships between intra-annual dynamics in F_{opt} and α and the vegetation indices for all sites combined were also analysed. In the analysis for all sites, data were normalised in order to avoid influence of spatial and inter-annual variability. Time series of ratios of F_{opt} and α (F_{opt_frac} and α_{frac}) against the annual peak values (F_{opt_peak} and α_{peak}; see below for calculation of annual peak values) were estimated for all sites:

$$F_{opt\_frac} = \frac{F_{opt}}{F_{opt\_peak}} \tag{7}$$

$$\alpha_{frac} = \frac{\alpha}{\alpha_{peak}} \tag{8}$$

The same standardisation procedure was used for all vegetation indices (VI_{frac}):

$$VI_{frac} = \frac{VI}{VI_{peak}} \tag{9}$$

where VI_{peak} is the annual peak values of the vegetation indices (14 days running mean with highest annual value). The coupling between α_{frac} and F_{opt_frac} and the different VI_{frac} were examined using Pearson correlation analysis for all sites.

Regression trees were used to fill gaps in the daily estimates of F_{opt} and α. One hundred tree sizes were chosen based on 100 cross validation runs, and these trees were then used for estimating F_{opt} and α following the method in De'ath and Fabricius (2000). We used SWC, VPD, T_{air}, PAR, and the vegetation index with strongest correlation with intra-annual dynamics as explanatory variables in the analysis. In the analysis for all sites, the same standardisation procedure as done for F_{opt}, α, and the vegetation indices was done for the hydrometeorological variables. The 100 F_{opt} and α output subsets from the regression trees were averaged and used for filling gaps in the times series of F_{opt} and α. From these time-series we estimated annual peak values of F_{opt} and α (F_{opt_peak} and α_{peak}) as the 14-day running mean with highest annual value. To investigate spatial and inter-annual variability in F_{opt} and α across the measurement sites of the Sahel, F_{opt_peak} and α_{peak} were correlated with the annual sum of P, yearly means of T_{air}, SWC, RH, VPD, R_g, annual peak values of biomass, soil nitrogen and C concentrations, C3/C4 ratio, and VI_{peak} using Pearson linear correlations.

2.4.2 Parameterisation and evaluation of the GPP model and evaluation of the MODIS GPP

Based on Eq. 1 and outcome of the statistical analysis previously described under subsection 2.4.1 (for results see subsect. 3.2), a model for estimating GPP across Sahel was created:

$$GPP = -F_{opt} \times (1 - e^{\left(\frac{-\alpha \times PAR}{F_{opt}}\right)}) \tag{10}$$

Firstly, F_{opt_peak} and α_{peak} were estimated spatially and inter-annually using linear regression functions fitted against the vegetation indices with strongest relationships to spatial and inter-annual variability in F_{opt_peak} and α_{peak} for all sites. Secondly, exponential regression functions were established for F_{opt_frac} and α_{frac} with the vegetation index with the strongest relationships to intra-annual variability of F_{opt_frac} and α_{frac} for all sites. By combining these relationships, F_{opt} and α can be calculated for any day of year and for any point in space across Sahel:

$$F_{opt} = F_{opt\_peak} \times F_{opt\_frac} = \left(k_{Fopt} \times NDVI_{peak} + m_{Fopt}\right)\left(n_{Fopt} \times e^{\left(l_{Fopt} \times RDVI_{frac}\right)}\right) \tag{11}$$

$$\alpha = \alpha_{peak} \times \alpha_{frac} = \left(k_{\alpha} \times RDVI_{peak} + m_{\alpha}\right)\left(n_{\alpha} \times e^{\left(l_{\alpha} \times RDVI_{frac}\right)}\right) \tag{12}$$

where k_{Fopt} and k_α are slopes and m_{Fopt} and m_α are intercepts of the linear regressions giving F_{opt_peak} and α_{peak}, respectively; l_{Fopt} and l_α are coefficients and n_{Fopt} and n_α are intercepts of the exponential regressions giving F_{opt_frac} and α_{frac}, respectively. Equation 11 and 12 were inserted into Eq. 10 and GPP were thereby estimated as:

$$GPP = -\left(F_{opt\_peak} \times F_{opt\_frac}\right) \times (1 - e^{\left(\frac{-\left(\alpha_{peak} \times \alpha_{frac}\right) \times PAR}{F_{opt\_peak} \times F_{opt\_frac}}\right)} = -\left(\left(k_{Fopt} \times NDVI_{peak} + m_{Fopt}\right)\left(n_{Fopt} \times e^{\left(l_{Fopt} \times RDVI_{frac}\right)}\right)\right) \times \left(1 - e^{\left(\frac{-\left(k_\alpha \times RDVI_{peak} + m_\alpha\right)\left(n_\alpha \times e^{\left(l_\alpha \times RDVI_{frac}\right)}\right) \times PAR}{\left(k_{Fopt} \times NDVI_{peak} + m_{Fopt}\right)\left(l_{Fopt} \times RDVI_{frac} + n_{Fopt}\right)}\right)}\right)) \quad (13)$$

A bootstrap simulation methodology with 200 iterations was used when fitting the least-square regression functions for parameterisation of the GPP model (Richter et al., 2012). For each of the iterations, some of the EC sites were included and some were left-out. The bootstrap simulations generated 200 sets of k_{Fopt}, k_α, m_{Fopt}, m_α, l_{Fopt}, l_α, n_{Fopt}, n_α, and coefficient of determination (R^2), from which the medians and the standard deviations were estimated. Possible errors (e.g. random sampling errors, aerosols, electrical sensor noise, filtering and gap-filling errors, clouds, and satellite sensor degradation) can be present in both the predictor and the response variables. Hence, we selected reduced major axis regressions to account for errors in both predictor and response variables when fitting the regression functions. The regression models were validated against the left-out sites within the bootstrap simulation methodology by calculating the root-mean-square-error (RMSE), and by fitting an ordinary least squares linear regression between modelled and independent variables.

Similarly, the MODIS GPP product (MOD17A2H, collection 6) was evaluated against independent GPP from the EC sites by calculating RMSE, and by fitting an ordinary least squares linear regression.

3 Results

3.1 Evaluation of the MODIS GPP product

There was a strong linear relationship between the MODIS GPP product (MOD17A2H; collection 6) and independent GPP (slope=0.17; intercept=0.11 g C m^{-2} d^{-1}; R^2=0.69; n=598). However, MOD17A2H strongly underestimated independent GPP (Fig. 2) resulting in high RMSE (2.69 g C m^{-2} d^{-1}). It can be seen that some points for the Kelma site were quite low for MOD17A2H, whereas they were relatively high for the independent GPP (Fig. 2). Kelma is an inundated Acacia forest located in a clay soil depression. These differentiated values were found in the beginning of the dry season, when the depression was still inundated, whereas the larger area was turning dry.

<Figure 2>

3.2 Intra-annual dynamics in photosynthetic capacity and quantum efficiency

Intra-annual dynamics in F_{opt} and α differed in amplitude, but were otherwise similar across the measurement sites in Sahel (Fig. 3). There was no green ground vegetation during the dry season, and the low photosynthetic activity was due to few evergreen trees. This resulted in low values for both F_{opt} and α during the dry season. The vegetation responded strongly to rainfall, and both F_{opt} and α increased during the early phase of the rainy season. Generally, F_{opt} peaked slightly earlier than α (average± 1 standard deviation: 7±10 days) (Fig. 3).

<Figure 3>

All vegetation indices described well intra-annual dynamics in F_{opt} for all sites (Table 2). $SIWSI_{12}$ had the highest correlation for all sites except Wankama Millet, where it was RDVI. When all sites were combined, all indices described well seasonality in F_{opt}, but RDVI had the strongest correlation (Table 2).

Intra-annual dynamics in α were also closely coupled to intra-annual dynamics in the vegetation indices for all sites (Table 2). For α, RDVI was the strongest index describing intra-annual dynamics, except for Wankama Fallow where it was EVI. When all sites were combined all indices described well intra-annual dynamics in α, but RDVI was still the index with strongest relationship (Table 2).

<Table 2>

The regression trees used for gap-filling explained well the intra-annual dynamics in F_{opt} and α for all sites (Table 3; Fig. S2 in Supplementary material). The regression trees explained intra-annual dynamics in F_{opt} better than in α, and multi-year sites were better predicted than single year sites (Fig. S2). The main explanatory variables coupled to intra-annual dynamics in F_{opt} for all sites across Sahel were in the order of RDVI, SWC, VPD, T_{air}, and PAR; and for α they were RDVI, SWC, VPD and T_{air} (Table 3). The strong relationship to SWC and VPD indicates drought stress during periods of low rainfall. For all sites across Sahel, incorporating hydrometeorological variables increased the ability to determine intra-annual dynamics in F_{opt} and α compared to the ordinary least squares linear regressions against vegetation indices (Table 2, data given as *r;* Table 3; Fig. 3 and Fig. S2). For all sites, incorporation of these variables increased R^2 from 0.81 to 0.87 and from 0.74 to 0.84, for F_{opt} and α respectively.

<Table 3>

3.3 Spatial and inter-annual dynamics in photosynthetic capacity and quantum efficiency

Large spatial and inter-annual variability in F_{opt_peak} and α_{peak} were found across the six measurement sites in Sahel; F_{opt_peak} ranged between 10.1 μmol CO_2 m^{-2} s^{-1} (Wankama Millet 2005) and 50.0 μmol CO_2 m^{-2} s^{-1} (Dahra 2010), and α_{peak} ranged between 0.020 μmol CO_2 μmol PAR^{-1} (Demokeya 2007) and 0.064 μmol CO_2 μmol PAR^{-1} (Dahra 2010) (Table 4). The average two week running mean peak values of F_{opt} and α for all sites were 26.4 μmol CO_2 m^{-2} s^{-1} and 0.040 μmol CO_2 μmol PAR^{-1}, respectively. All vegetation indices determined well spatial and inter-annual dynamics in F_{opt_peak} and α_{peak} (Table 5). $NDVI_{peak}$ was most closely coupled with F_{opt_peak} whereas $RDVI_{peak}$ was closest coupled with α_{peak} (Fig. 4). F_{opt_peak} also correlated well with peak dry weight biomass, C content in the soil, and RH, whereas α_{peak} also correlated well with peak dry weight biomass, and C content in the soil (Table 5).

<Table 4>

<Table 5>

<Figure 4>

3.4 Spatially extrapolated photosynthetic capacity, quantum efficiency, and gross primary production across Sahel and evaluation of the GPP model

The spatially extrapolated F_{opt}, α and GPP averaged over Sahel for 2001-2014 were 22.5±1.7 μmol CO_2 m^{-2} s^{-1}, 0.030±0.002 μmol CO_2 μmol PAR^{-1}, and 736±39 g C m^{-2} y^{-1}, respectively. At regional scale it can be seen that F_{opt}, α, and GPP decreased substantially with latitude (Fig. 5). Highest values were found in south-eastern Senegal, western Mali, in parts of southern Sudan and on the border between Sudan and South Sudan. Lowest values were found along the northernmost parts of Sahel on the border to Sahara in Mauritania, in northern Mali, and in northern Niger.

Modelled GPP was similar to independent GPP on average, and there was a strong linear relationship between modelled GPP and independent GPP for all sites (Fig. 6; Table 6). However, when separating the evaluation between measurement sites, it can be seen that the model reproduced some sites better than others (Fig. 7; Table 6). Wankama Millet was generally overestimated whereas the model worked well on average for Demokeya but underestimated high values (Fig. 7; Table 6). Variability of independent GPP at the other sites was well reproduced by the model (Fig. 7; Table 6). The final parameters of the GPP model (Eq. 13) are given in Table 7.

<Figure 5>

<Figure 6>

<Figure 7>

< Table 6>

< Table 7>

4 Discussions

Our hypothesis that vegetation indices closely related to equivalent water thickness (SIWSI) would be most strongly coupled with intra-annual dynamics in F_{opt} and α was not rejected for F_{opt}, since this was the case for all sites except for Wankama Millet (Table 2). However, our hypothesis was rejected for α, since it was more closely related to vegetation indices related to chlorophyll abundance (RDVI and EVI). In Sahel, soil moisture conditions in the early rainy season are important for vegetation growth and during this phase vegetation is especially vulnerable to drought conditions (Rockström and de Rouw, 1997; Tagesson et al., 2016a; Mbow et al., 2013). Photosynthetic capacity (F_{opt}) peaked earlier in the rainy season than α did (Fig. 3), thereby explaining the close relationship of F_{opt} to SIWSI. Leaf area index increased over the growing season and leaf area index is closely coupled with vegetation indices related to chlorophyll abundance (Tagesson et al., 2009). The increase in leaf area index increased canopy level quantum efficiency (α), which thereby explains the closer relationship of α to RDVI.

Our hypothesis that vegetation indices closely related to chlorophyll abundance would be most strongly coupled with spatial and inter-annual dynamics in F_{opt} and α was not rejected for either F_{opt} or α; NDVI, EVI, and RDVI all had close correlation with spatial and inter-annual dynamics in F_{opt} and α (Table 5). However, it was surprising that $NDVI_{peak}$ had the strongest correlation with spatial and inter-annual variability for F_{opt} (Table 5). Both EVI and RDVI should be less sensitive to saturation effects than NDVI (Huete et al., 2002; Roujean and Breon, 1995), and based on this it can be assumed that peak values of these indices should have stronger relationships to peak values of F_{opt} and α. However, vegetation indices with a high sensitivity to changes in green biomass at high biomass loads, gets less sensitive to green biomass changes at low biomass loads (Huete et al., 2002). Peak leaf area index for ecosystems across Sahel is generally ~2 or less, whereas the saturation issue of NDVI generally starts at an leaf area index of about 2-5 (Haboudane et al., 2004).

The F_{opt_peak} estimates from Agoufou, Demokeya, and the Wankama sites were similar whereas Dahra and Kelma values were high in relation to previously reported canopy-scale F_{opt_peak} from Sahel (~-8 to -23 μmol m^{-2} sec^{-1}) (Hanan et al., 1998; Merbold et al., 2009; Moncrieff et al., 1997; Boulain et al., 2009; Levy et al., 1997; Monteny et al., 1997). These previous studies reported much lower F_{opt} at canopy scale than at leaf scale (e.g. Levy et al. (1997): 10 vs. 44 μmol m^{-2} sec^{-1}; Boulain et al. (2009): 8 vs. 50 μmol m^{-2} sec^{-1}). Leaf area index at Dahra and Kelma peaked at 2.1 and 2.7, respectively (Timouk et al., 2009; Tagesson et al., 2015a), and it was substantially higher than at the above-mentioned sites. A possible explanation to high F_{opt} estimates at Dahra and Kelma could thereby be the higher leaf area index. Tagesson et al. (2016b) performed a quality check of the EC data due to the high net CO_2 exchange measured at the Dahra field site and explained the high values by a combination of moderately dense herbaceous C4 ground vegetation, high soil nutrient availability, and a grazing pressure resulting in compensatory growth and fertilization effects. Another possible explanation could be that the West African Monsoon bring a humid layer of surface air from the Atlantic, possibly increasing vegetation production for the most western part of Sahel (Tagesson et al., 2016a).

Our model substantially overestimated GPP for Wankama Millet (Fig. 7f). Being a crop field, this site differed from the other studied sites by its species composition, ecosystem structure, as well as land and vegetation management. Crop fields in southwestern Niger are generally characterized by a rather low production resulting from decreased fertility and soil loss caused by intensive land use (Cappelaere et al., 2009)**.** These specifics of the Wankama Millet site may cause the model parameterised with observations from the other study sites without this strong anthropogenic influence to overestimate GPP at this site. Similar results were found by Boulain et al. (2009) when applying an up-scaling model using leaf area index for Wankama Millet and Wankama Fallow. It worked well for Wankama fallow whereas it was less conclusive for Wankama Millet. The main explanation was low leaf area index in millet fields because of a low density of millet stands due to agricultural practice. There is extensive savanna clearing for food production in Sahel (Leblanc et al., 2008; Boulain et al., 2009; Cappelaere et al., 2009). To further understand impacts of this land cover change on vegetation production and land atmosphere exchange processes, it is of urgent need for more study sites covering cropped areas in this region.

In Demokeya, GPP was slightly underestimated for the year 2008 (Fig. 7c) because modelled F_{opt} was much lower than the actual measured value in 2008 (the thick black line in Fig. 4). An improvement of the model could be to incorporate some parameters that constrain or enhance F_{opt} depending on environmental stress. Indeed, the regression tree analysis indicated that incorporating hydrometeorological variables increased the ability to predict both F_{opt} and α. On the other hand, for spatial upscaling purposes, it has been shown that including modelled hydrometeorological constraints on LUE decreases the ability to predict vegetation production due to the incorporated uncertainty in these modelled variables (Fensholt et al., 2006; Ma et al., 2014). For spatial upscaling to regional scales it is therefore better to simply use relationships to EO data. This is particularly the case for Sahel, one of the largest dryland areas in the world that includes only a few sites of hydrometeorological observations.

The pattern seen in the spatially explicit GPP budgets (Fig. 5c) may be influenced by a range of biophysical and anthropogenic factors. The clear North-South gradient is expected given the strong North-South rainfall gradient in Sahel. The West African Monsoon mentioned above could also be an explanation to high GPP values in the western part of Sahel, where values were relatively high in relation to GPP at similar latitudes in the central and eastern Sahel (Fig. 5c). The areas with highest GPP are sparsely populated woodlands or shrubby savanna with a relatively dense tree cover (Brandt et al., 2016). However, the produced maps should be used with caution as they are based on up-scaling of the only six available EC sites that exist in the region; especially given the issues related to the cropped fields discussed above. Still, the average GPP budget for the entire Sahel 2001-2014 was close to an average annual GPP budget as estimated for these six sites (692±89 g C m^{-2} y^{-1}) (Tagesson et al., 2016a). The range of GPP budgets in Fig. 5c is also similar to previous annual GPP budgets reported from other savanna areas across the world (Veenendaal et al., 2004; Chen et al., 2003; Kanniah et al., 2010; Chen et al., 2016).

Although MOD17A2 GPP has previously been shown to relatively well capture GPP in several different ecosystems (Turner et al., 2006; Turner et al., 2005; Heinsch et al., 2006; Sims et al., 2006; Kanniah et al., 2009), it has been shown to be underestimated for others (Coops et al., 2007; Gebremichael and Barros, 2006; Sjöström et al., 2013). GPP of Sahelian drylands have not been well captured by MOD17A2 (Sjöström et al., 2013; Fensholt et al., 2006), and as we have shown, this underestimation persists in the latest MOD17A2H GPP (collection 6) product (Fig. 2). The main reason for this pronounced underestimation is that maximum LUE is set to 0.84 g C MJ^{-1} (open shrubland; Demokeya) and 0.86 g C MJ^{-1} (grassland; Agoufou, Dahra, Kelma; Wankama Millet and Wankama Fallow) in the BPLUT, i.e. much lower than maximum LUE measured at the Sahelian measurement sites of this study (average: 2.47 g C MJ^{-1}; range: 1.58-3.50 g C MJ^{-1}) (Sjöström et al., 2013; Tagesson et al., 2015a), a global estimate of ~1.5 g C MJ^{-1} (Garbulsky et al., 2010), and a savanna site in Australia (1.26 g C MJ^{-1}) (Kanniah et al., 2009).

Several dynamic global vegetation models have been used for decades to quantify GPP at different spatial and temporal scales (Dickinson, 1983; Sellers et al., 1997). These models are generally based on the photosynthesis model by Farquhar et al. (1980), a model particularly sensitive to uncertainty in photosynthetic capacity (Zhang et al., 2014). This and several previous studies have shown that both photosynthetic capacity and efficiency (both α and LUE) can vary considerably between seasons as well as spatially, and both within and between vegetation types (Eamus et al., 2013; Garbulsky et al., 2010; Ma et al., 2014; Tagesson et al., 2015a). This variability is difficult to estimate using broad values based on land cover classes, yet most models apply a constant value which can cause substantial inaccuracies in the estimates of seasonal and spatial variability in GPP. This is particularly a problem in savannas that comprises several plant functional types (C3 and C4 species, and a large variability in tree/herbaceous vegetation fractions) (Scholes and Archer, 1997). This study indicates the strong applicability of EO as a tool for parameterising spatially explicit estimates of plant physiological variables, which could improve our ability to simulate GPP. Spatially explicit estimates of GPP at a high temporal and spatial resolution are essential for environmental change studies in Sahel and make a major asset for the analysis of changes in GPP, its relationship to climatic change and anthropogenic forcing, and estimations of ecosystem processes and biochemical and hydrological cycles.

Acknowledgements Data is available from Fluxnet (http://fluxnet.ornl.gov) and CarboAfrica (http://www.carboafrica.net/index en.asp). Data for the Mali and Niger sites were made available by the AMMA-CATCH regional observatory (www.amma-catch.org), which is funded by the French Institut de Recherche pour le Développement (IRD) and Institut National des Sciences de l'Univers (INSU). The project was funded by the Danish Council for Independent Research (DFF) Sapere Aude programme. Faculty of Science, Lund University supported the Dahra and Demokeya measurements with an infrastructure grant. Ardö received support from the Swedish National Space Board.

References

Abdi, A., Seaquist, J., Tenenbaum, D., Eklundh, L., and Ardö, J.: The supply and demand of net primary production in the Sahel, Environ. Res. Lett., 9, 094003, doi:10.1088/1748-9326/9/9/094003, 2014.

Ahlström, A., Raupach, M. R., Schurgers, G., Smith, B., Arneth, A., Jung, M., Reichstein, M., Canadell, J. G., Friedlingstein, P., Jain, A. K., Kato, E., Poulter, B., Sitch, S., Stocker, B. D., Viovy, N., Wang, Y. P., Wiltshire, A., Zaehle, S., and Zeng, N.: The dominant role of semi-arid ecosystems in the trend and variability of the land CO_2 sink, Science, 348, 895-899, 10.1126/science.aaa1668, 2015.

Baldocchi, D., Falge, E., Gu, L., Olson, R., Hollinger, D., Running, S., Anthoni, P., Bernhofer, C., Davis, K., Evans, R., Fuentes, J., Goldstein, A., Katul, G., Law, B., Lee, X., Malhi, Y., Meyers, T., Munger, W., Oechel, W., Paw, K. T., Pilegaard, K., Schmid, H. P., Valentini, R., Verma, S., Vesala, T., Wilson, K., and Wofsy, S.: FLUXNET: A New Tool to Study the Temporal and Spatial Variability of Ecosystem–Scale Carbon Dioxide, Water Vapor, and Energy Flux Densities, Bull. Am. Meteorol. Soc., 82, 2415-2434, 10.1175/1520-0477(2001)082<2415:fantts>2.3.co;2, 2001.

Boulain, N., Cappelaere, B., Ramier, D., Issoufou, H. B. A., Halilou, O., Seghieri, J., Guillemin, F., Oï, M., Gignoux, J., and Timouk, F.: Towards an understanding of coupled physical and biological processes in the cultivated Sahel – 2. Vegetation and carbon dynamics, J. Hydrol., 375, 190-203, 10.1016/j.jhydrol.2008.11.045, 2009.

Brandt, M., Hiernaux, P., Rasmussen, K., Mbow, C., Kergoat, L., Tagesson, T., Ibrahim, Y. Z., Wélé, A., Tucker, C. J., and Fensholt, R.: Assessing woody vegetation trends in Sahelian drylands using MODIS based seasonal metrics, Remote Sens. Environ., 183, 215-225, http://dx.doi.org/10.1016/j.rse.2016.05.027, 2016.

Broge, N. H., and Leblanc, E.: Comparing prediction power and stability of broadband and hyperspectral vegetation indices for estimation of green leaf area index and canopy chlorophyll density, Remote Sens. Environ., 76, 156-172, http://dx.doi.org/10.1016/S0034-4257(00)00197-8, 2001.

Cannell, M., and Thornley, J.: Temperature and CO_2 Responses of Leaf and Canopy Photosynthesis: a Clarification using the Non-rectangular Hyperbola Model of Photosynthesis, Ann. Bot., 82, 883-892, 1998.

Cappelaere, B., Descroix, L., Lebel, T., Boulain, N., Ramier, D., Laurent, J. P., Favreau, G., Boubkraoui, S., Boucher, M., Bouzou Moussa, I., Chaffard, V., Hiernaux, P., Issoufou, H. B. A., Le Breton, E., Mamadou, I., Nazoumou, Y., Oi, M., Ottlé, C., and Quantin, G.: The AMMA-CATCH experiment in the cultivated Sahelian area of south-west Niger – Investigating water cycle response to a fluctuating climate and changing environment, J. Hydrol., 375, 34-51, 10.1016/j.jhydrol.2009.06.021, 2009.

Chen, C., Cleverly, J., and Zhang, L.: Modelling Seasonal and Inter-annual Variations in Carbon and Water Fluxes in an Arid-Zone Acacia Savanna Woodland, 1981–2012, Ecosystems, 19, 625-644, 2016.

Chen, X., Hutley, L., and Eamus, D.: Carbon balance of a tropical savanna of northern Australia., Oecologia, 137, 405-416, 2003.

Coops, N. C., Black, T. A., Jassal, R. S., Trofymow, J. A., and Morgenstern, K.: Comparison of MODIS, eddy covariance determined and physiologically modelled gross primary production (GPP) in a Douglas-fir forest stand, Remote Sens. Environ., 107, 385-401, http://dx.doi.org/10.1016/j.rse.2006.09.010, 2007.

Dardel, C., Kergoat, L., Hiernaux, P., Mougin, E., Grippa, M., and Tucker, C. J.: Re-greening Sahel: 30 years of remote sensing data and field observations (Mali, Niger), Remote Sens. Environ., 140, 350-364, http://dx.doi.org/10.1016/j.rse.2013.09.011, 2014.

De'ath, G., and Fabricius, K. E.: Classification and regression trees: A powerful yet simple technique for ecological data analysis, Ecology, 81, 3178-3192, 10.2307/177409, 2000.

de Ridder, N., Stroosnijder, L., and Cisse, A. M.: Productivity of Sahelian rangelands : a study of the soils, the vegetations and the exploitation of that natural resource, PPS course book. Primary Production in the Sahel, Agricultural University, Wageningen, 1982.

Dee, D. P., Uppala, S. M., Simmons, A. J., Berrisford, P., Poli, P., Kobayashi, S., Andrae, U., Balmaseda, M. A., Balsamo, G., Bauer, P., Bechtold, P., Beljaars, A. C. M., van de Berg, L., Bidlot, J., Bormann, N., Delsol, C., Dragani, R., Fuentes, M., Geer, A. J., Haimberger, L., Healy, S. B., Hersbach, H., Hólm, E. V., Isaksen, L., Kållberg, P., Köhler, M., Matricardi, M., McNally, A. P., Monge-Sanz, B. M., Morcrette, J. J., Park, B. K., Peubey, C., de Rosnay, P., Tavolato, C., Thépaut, J. N., and Vitart, F.: The ERA-Interim reanalysis: configuration and performance of the data assimilation system, Q. J. Roy. Meteor. Soc., 137, 553-597, 10.1002/qj.828, 2011.

Dickinson, R. E.: Land Surface Processes and Climate—Surface Albedos and Energy Balance, in: Advances in Geophysics, edited by: Barry, S., Elsevier, 305-353, 1983.

Eamus, D., Cleverly, J., Boulain, N., Grant, N., Faux, R., and Villalobos-Vega, R.: Carbon and water fluxes in an arid-zone Acacia savanna woodland: An analyses of seasonal patterns and responses to rainfall events, Agric. For. Meteorol., 182–183, 225-238, http://dx.doi.org/10.1016/j.agrformet.2013.04.020, 2013.

ECMWF: ERA Interim Daily: http://apps.ecmwf.int/datasets/data/interim-full-daily/levtype=sfc/, access: 04-04-2016, 2016a.

ECMWF: ERA-Interim: surface photosynthetically active radiation (surface PAR) values are too low https://software.ecmwf.int/wiki/display/CKB/ERA-Interim%3A+surface+photosynthetically+active+radiation+%28surface+PAR%29+values+are+too+low, access: 7 November, 2016b.

Falge, E., Baldocchi, D., Olson, R., Anthoni, P., Aubinet, M., Bernhofer, C., Burba, G., Ceulemans, R., Clement, R., Dolman, H., Granier, A., Gross, P., Grunwald, T., Hollinger, D., Jensen, N. O., Katul, G., Keronen, P., Kowalski, A., Lai, C. T., Law, B. E., Meyers, T., Moncrieff, J. B., Moors, E., Munger, J. W., Pilegaard, K., Rannik, U., Rebmann, C., Suyker, A., Tenhunen, J., Tu, K., Verma, S., Vesala, T., Wilson, K., and Wofsy, S.: Gap filling strategies for defensible annual sums of net ecosystem exchange, Agric. For. Meteorol., 107, 43-69, 2001.

Farquhar, G. D., Caemmerer, S., and Berry, J. A.: A biochemical model of photosynthetic CO_2 assimilation in leaves of C3 plants, Planta, 149, 78-90, 1980.

Fensholt, R., and Sandholt, I.: Derivation of a shortwave infrared water stress index from MODIS near- and shortwave infrared data in a semiarid environment, Remote Sens. Environ., 87, 111-121, http://dx.doi.org/10.1016/j.rse.2003.07.002, 2003.

Fensholt, R., Sandholt, I., Rasmussen, M. S., Stisen, S., and Diouf, A.: Evaluation of satellite based primary production modelling in the semi-arid Sahel, Remote Sens. Environ., 105, 173-188, 10.1016/j.rse.2006.06.011, 2006.

Fensholt, R., Rasmussen, K., Kaspersen, P., Huber, S., Horion, S., and Swinnen, E.: Assessing Land Degradation/Recovery in the African Sahel from Long-Term Earth Observation Based Primary Productivity and Precipitation Relationships, Remote Sensing, 5, 664-686, 2013.

Garbulsky, M. F., Peñuelas, J., Papale, D., Ardö, J., Goulden, M. L., Kiely, G., Richardson, A. D., Rotenberg, E., Veenendaal, E. M., and Filella, I.: Patterns and controls of the variability of radiation use efficiency and primary productivity across terrestrial ecosystems, Global Ecol. Biogeogr., 19, 253-267, 10.1111/j.1466-8238.2009.00504.x, 2010.

Gates, D. M., Keegan, H. J., Schleter, J. C., and Weidner, V. R.: Spectral Properties of Plants, Appl. Optics, 4, 11-20, 1965.

Gebremichael, M., and Barros, A. P.: Evaluation of MODIS Gross Primary Productivity (GPP) in tropical monsoon regions, Remote Sens. Environ., 100, 150-166, http://dx.doi.org/10.1016/j.rse.2005.10.009, 2006.

Haboudane, D., Miller, J. R., Pattey, E., Zarco-Tejada, P. J., and Strachan, I. B.: Hyperspectral vegetation indices and novel algorithms for predicting green LAI of crop canopies: Modeling and validation in the context of precision agriculture, Remote Sens. Environ., 90, 337-352, http://dx.doi.org/10.1016/j.rse.2003.12.013, 2004.

Hanan, N., Kabat, P., Dolman, J., and Elbers, J. A. N.: Photosynthesis and carbon balance of a Sahelian fallow savanna, Global Change Biol., 4, 523-538, 1998.

Heinsch, F. A., Maosheng, Z., Running, S. W., Kimball, J. S., Nemani, R. R., Davis, K. J., Bolstad, P. V., Cook, B. D., Desai, A. R., Ricciuto, D. M., Law, B. E., Oechel, W. C., Hyojung, K., Hongyan, L., Wofsy, S. C., Dunn, A. L., Munger, J. W., Baldocchi, D. D., Liukang, X., Hollinger, D. Y., Richardson, A. D., Stoy, P. C., Siqueira, M. B. S., Monson, R. K., Burns, S. P., and Flanagan, L. B.: Evaluation of remote sensing based terrestrial productivity from MODIS using regional tower eddy flux network observations, IEEE T. Geosci. Remote, 44, 1908-1925, 10.1109/TGRS.2005.853936, 2006.

Hickler, T., Eklundh, L., Seaquist, J. W., Smith, B., Ardö, J., Olsson, L., Sykes, M. T., and Sjöström, M.: Precipitation controls Sahel greening trend, Geophys. Res. Lett., 32, L21415, doi:10.1029/2005GL024370, 2005.

Huber, S., Tagesson, T., and Fensholt, R.: An automated field spectrometer system for studying VIS, NIR and SWIR anisotropy for semi-arid savanna, Remote Sens. Environ., 152, 547–556, 2014.

Huete, A., Didan, K., Miura, T., Rodriguez, E. P., Gao, X., and Ferreira, L. G.: Overview of the radiometric and biophysical performance of the MODIS vegetation indices, Remote Sens. Environ., 83, 195–213, 2002.

Ide, R., Nakaji, T., and Oguma, H.: Assessment of canopy photosynthetic capacity and estimation of GPP by using spectral vegetation indices and the light-response function in a larch forest, Agric. For. Meteorol., 150, 389-398, 2010.

Inoue, Y., Penuelas, J., Miyata, A., and Mano, M.: Normalized difference spectral indices for estimating photosynthetic efficiency and capacity at a canopy scale derived from hyperspectral and CO_2 flux measurements in rice, Remote Sens. Environ., 112, 156-172, 2008.

Jin, H., and Eklundh, L.: A physically based vegetation index for improved monitoring of plant phenology, Remote Sens. Environ., 152, 512-525, http://dx.doi.org/10.1016/j.rse.2014.07.010, 2014.

Kanniah, K. D., Beringer, J., Hutley, L. B., Tapper, N. J., and Zhu, X.: Evaluation of Collections 4 and 5 of the MODIS Gross Primary Productivity product and algorithm improvement at a tropical savanna site in northern Australia, Remote Sens. Environ., 113, 1808-1822, http://dx.doi.org/10.1016/j.rse.2009.04.013, 2009.

Kanniah, K. D., Beringer, J., and Hutley, L. B.: The comparative role of key environmental factors in determining savanna productivity and carbon fluxes: A review, with special reference to Northern Australia, Progress in Physical Geography, 34, 459-490, 2010.

Kergoat, L., Lafont, S., Arneth, A., Le Dantec, V., and Saugier, B.: Nitrogen controls plant canopy light-use efficiency in temperate and boreal ecosystems, J. Geophys. Res., 113, 1-19, 10.1029/2007JG000676, 2008.

Leblanc, M. J., Favreau, G., Massuel, S., Tweed, S. O., Loireau, M., and Cappelaere, B.: Land clearance and hydrological change in the Sahel: SW Niger, Global Planet. Change, 61, 135-150, http://dx.doi.org/10.1016/j.gloplacha.2007.08.011, 2008.

Levy, P. E., Moncrieff, J. B., Massheder, J. M., Jarvis, P. G., Scott, S. L., and Brouwer, J.: CO2 fluxes at leaf and canopy scale in millet, fallow and tiger bush vegetation at the HAPEX-Sahel southern super-site, J. Hydrol., 188, 612-632, http://dx.doi.org/10.1016/S0022-1694(96)03195-2, 1997.

Ma, X., Huete, A., Yu, Q., Restrepo-Coupe, N., Beringer, J., Hutley, L. B., Kanniah, K. D., Cleverly, J., and Eamus, D.: Parameterization of an ecosystem light-use-efficiency model for predicting savanna GPP using MODIS EVI, Remote Sens. Environ., 154, 253-271, http://dx.doi.org/10.1016/j.rse.2014.08.025, 2014.

Mayaux, P., Bartholomé, E., Massart, M., Cutsem, C. V., Cabral, A., Nonguierma, A., Diallo, O., Pretorius, C., Thompson, M., Cherlet, M., Pekel, J.-F., Defourny, P., Vasconcelos, M., Gregorio, A.

D., S.Fritz, Grandi, G. D., C..Elvidge, P.Vogt, and Belward, A.: EUR 20665 EN –A Land-cover map of Africa, edited by: Centre', E. C. J. R., European Commisions Joint Research Centre, Luxembourg, 38 pp., 2003.

Mbow, C., Fensholt, R., Rasmussen, K., and Diop, D.: Can vegetation productivity be derived from greenness in a semi-arid environment? Evidence from ground-based measurements, J. Arid Environ., 97, 56-65, http://dx.doi.org/10.1016/j.jaridenv.2013.05.011, 2013.

Merbold, L., Ardö, J., Arneth, A., Scholes, R. J., Nouvellon, Y., de Grandcourt, A., Archibald, S., Bonnefond, J. M., Boulain, N., Brueggemann, N., Bruemmer, C., Cappelaere, B., Ceschia, E., El-Khidir, H. A. M., El-Tahir, B. A., Falk, U., Lloyd, J., Kergoat, L., Le Dantec, V., Mougin, E., Muchinda, M., Mukelabai, M. M., Ramier, D., Roupsard, O., Timouk, F., Veenendaal, E. M., and Kutsch, W. L.: Precipitation as driver of carbon fluxes in 11 African ecosystems, Biogeosciences, 6, 1027-1041, 10.5194/bg-6-1027-2009, 2009.

Moncrieff, J. B., Monteny, B., Verhoef, A., Friborg, T., Elbers, J., Kabat, P., de Bruin, H., Soegaard, H., Jarvis, P. G., and Taupin, J. D.: Spatial and temporal variations in net carbon flux during HAPEX-Sahel, J. Hydrol., 188–189, 563-588, 10.1016/s0022-1694(96)03193-9, 1997.

Monteith, J. L.: Solar radiation and productivity in tropical ecosystems, J. Appl. Ecol., 9, 747-766, 1972.

Monteith, J. L.: Climate and the efficiency of crop production in Britain, Philos. Trans. Roy. Soc. B., 281, 277-294, 1977.

Monteny, B. A., Lhomme, J. P., Chehbouni, A., Troufleau, D., Amadou, M., Sicot, M., Verhoef, A., Galle, S., Said, F., and Lloyd, C. R.: The role of the Sahelian biosphere on the water and the CO2 cycle during the HAPEX-Sahel experiment, J. Hydrol., 188, 516-535, http://dx.doi.org/10.1016/S0022-1694(96)03191-5, 1997.

Mutanga, O., and Skidmore, A. K.: Narrow band vegetation indices overcome the saturation problem in biomass estimation, Int. J. Remote Sens., 25, 3999-4014, 10.1080/01431160310001654923, 2004.

NASA: Reverb ECHO: http://reverb.echo.nasa.gov/reverb/, access: June 2016, 2016.

Papale, D., Reichstein, M., Aubinet, M., Canfora, E., Bernhofer, C., Kutsch, W., Longdoz, B., Rambal, S., Valentini, R., Vesala, T., and Yakir, D.: Towards a standardized processing of Net Ecosystem Exchange measured with eddy covariance technique: algorithms and uncertainty estimation, Biogeosciences, 3, 571-583, 10.5194/bg-3-571-2006, 2006.

Paruelo, J. M., Garbulsky, M. F., Guerschman, J. P., and Jobbágy, E. G.: Two decades of Normalized Difference Vegetation Index changes in South America: identifying the imprint of global change, Int. J. Remote Sens., 25, 2793-2806, 10.1080/01431160310001619526, 2004.

Poulter, B., Frank, D., Ciais, P., Myneni, R. B., Andela, N., Bi, J., Broquet, G., Canadell, J. G., Chevallier, F., Liu, Y. Y., Running, S. W., Sitch, S., and van der Werf, G. R.: Contribution of semi-arid ecosystems to interannual variability of the global carbon cycle, Nature, 509, 600-603, 10.1038/nature13376, 2014.

Prince, S. D., Kerr, Y. H., Goutorbe, J. P., Lebel, T., Tinga, A., Bessemoulin, P., Brouwer, J., Dolman, A. J., Engman, E. T., Gash, J. H. C., Hoepffner, M., Kabat, P., Monteny, B., Said, F., Sellers, P., and Wallace, J.: Geographical, biological and remote sensing aspects of the hydrologic atmospheric pilot experiment in the sahel (HAPEX-Sahel), Remote Sens. Environ., 51, 215-234, http://dx.doi.org/10.1016/0034-4257(94)00076-Y, 1995.

Qi, J., Chehbouni, A., Huete, A. R., Kerr, Y. H., and Sorooshian, S.: A modified soil adjusted vegetation index, Remote Sens. Environ., 48, 119-126, 1994.

Richter, K., Atzberger, C., Hank, T. B., and Mauser, W.: Derivation of biophysical variables from Earth observation data: validation and statistical measures, J. Appl. Remote Sens., 6, 063557, 10.1117/1.JRS.6.063557, 2012.

Rietkerk, M., Ketner, P., Stroosnijder, L., and Prins, H. H. T.: Sahelian rangeland development; a catastrophe?, J. Range Manage., 49, 512-519, 1996.
Rockström, J., and de Rouw, A.: Water, nutrients and slope position in on-farm pearl millet cultivation in the Sahel, Plant Soil, 195, 311-327, 10.1023/A:1004233303066, 1997.
Roujean, J.-L., and Breon, F.-M.: Estimating PAR absorbed by vegetation from bidirectional reflectance measurements, Remote Sens. Environ., 51, 375-384, http://dx.doi.org/10.1016/0034-4257(94)00114-3, 1995.
Rouse, J. W., Haas, R. H., Schell, J. A., Deering, D. W., and Harlan, J. C.: Monitoring the Vernal Advancement of Retrogradation of Natural Vegetation, Type III, Final Report, Greenbelt, MD, 1974.
Ruimy, A., Saugier, B., and Dedieu, G.: Methodology for the estimation of terrestrial net primary production from remotely sensed data., J. Geophys. Res., 99, 5263-5283., 1994.
Running, S. W., Nemani, R. R., Heinsch, F. A., Zhao, M., Reeves, M., and Hashimoto, H.: A Continuous Satellite-Derived Measure of Global Terrestrial Primary Production, BioScience, 54, 547-560, 10.1641/0006-3568(2004)054[0547:ACSMOG]2.0.CO;2, 2004.
Running, S. W., and Zhao, M.: User's Guide. Daily GPP and Annual NPP (MOD17A2/A3) Products NASA Earth Observing System MODIS Land Algorithm. Version 3.0 For Collection 6., University of Montana, USA, NASA, 2015.
Scholes, R. J., and Archer, S. R.: Tree-grass interactions in savannas, Annual Review of Ecology and Systematics, 28, 517-544, 1997.
Sellers, P. J., Dickinson, R. E., Randall, D. A., Betts, A. K., Hall, F. G., Berry, J. A., Collatz, G. J., Denning, A. S., Mooney, H. A., Nobre, C. A., Sato, N., Field, C. B., and Henderson-Sellers, A.: Modeling the Exchanges of Energy, Water, and Carbon Between Continents and the Atmosphere, Science, 275, 502-509, 10.1126/science.275.5299.502, 1997.
Sims, D. A., Rahman, A. F., Cordova, V. D., El-Masri, B. Z., Baldocchi, D. D., Flanagan, L. B., Goldstein, A. H., Hollinger, D. Y., Misson, L., Monson, R. K., Oechel, W. C., Schmid, H. P., Wofsy, S. C., and Xu, L.: On the use of MODIS EVI to assess gross primary productivity of North American ecosystems, J. Geophys. Res., 111, G04015, 10.1029/2006JG000162, 2006.
Sjöström, M., Ardö, J., Eklundh, L., El-Tahir, B. A., El-Khidir, H. A. M., Hellström, M., Pilesjö, P., and Seaquist, J.: Evaluation of satellite based indices for gross primary production estimates in a sparse savanna in the Sudan, Biogeosciences, 6, 129-138, 2009.
Sjöström, M., Zhao, M., Archibald, S., Arneth, A., Cappelaere, B., Falk, U., de Grandcourt, A., Hanan, N., Kergoat, L., Kutsch, W., Merbold, L., Mougin, E., Nickless, A., Nouvellon, Y., Scholes, R. J., Veenendaal, E. M., and Ardö, J.: Evaluation of MODIS gross primary productivity for Africa using eddy covariance data, Remote Sens. Environ., 131, 275-286, http://dx.doi.org/10.1016/j.rse.2012.12.023, 2013.
Tagesson, T., Eklundh, L., and Lindroth, A.: Applicability of leaf area index products for boreal regions of Sweden, Int. J. Remote Sens., 30, 5619–5632, 2009.
Tagesson, T., Fensholt, R., Cropley, F., Guiro, I., Horion, S., Ehammer, A., and Ardö, J.: Dynamics in carbon exchange fluxes for a grazed semi-arid savanna ecosystem in West Africa, Agr. Ecosyst. Environ., 205, 15-24, http://dx.doi.org/10.1016/j.agee.2015.02.017, 2015a.
Tagesson, T., Fensholt, R., Guiro, I., Rasmussen, M. O., Huber, S., Mbow, C., Garcia, M., Horion, S., Sandholt, I., Rasmussen, B. H., Göttsche, F. M., Ridler, M.-E., Olén, N., Olsen, J. L., Ehammer, A., Madsen, M., Olesen, F. S., and Ardö, J.: Ecosystem properties of semi-arid savanna grassland in West Africa and its relationship to environmental variability, Global Change Biol., 21, 250-264, doi: 10.1111/gcb.12734, 2015b.

Tagesson, T., Fensholt, R., Huber, S., Horion, S., Guiro, I., Ehammer, A., and Ardö, J.: Deriving seasonal dynamics in ecosystem properties of semi-arid savannas using in situ based hyperspectral reflectance, Biogeosciences, 12, 4621-4635, doi:10.5194/bg-12-4621-2015, 2015c.

Tagesson, T., Fensholt, R., Cappelaere, B., E., M., Horion, S., L., K., Nieto, H., Ehammer, A., Demarty, J., and Ardö, J.: Spatiotemporal variability in carbon exchange fluxes across the Sahel Agric. For. Meteorol., 226–227, 108-118, 2016a.

Tagesson, T., Fensholt, R., Guiro, I., Cropley, F., Horion, S., Ehammer, A., and Ardö, J.: Very high carbon exchange fluxes for a grazed semi-arid savanna ecosystem in West Africa, Danish Journal of Geography, 116, 93-109, http://dx.doi.org/10.1080/00167223.2016.1178072 2016b.

Timouk, F., Kergoat, L., Mougin, E., Lloyd, C. R., Ceschia, E., Cohard, J. M., Rosnay, P. d., Hiernaux, P., Demarez, V., and Taylor, C. M.: Response of surface energy balance to water regime and vegetation development in a Sahelian landscape, J. Hydrol., 375, 12-12, 10.1016/j.jhydrol.2009.04.022, 2009.

Turner, D. P., Ritts, W. D., Cohen, W. B., Maeirsperger, T. K., Gower, S. T., Kirschbaum, A. A., Running, S. W., Zhao, M., Wofsy, S. C., Dunn, A. L., Law, B. E., Campbell, J. L., Oechel, W. C., Kwon, H. J., Meyers, T. P., Small, E. E., Kurc, S. A., and Gamon, J. A.: Site-level evaluation of satellite-based global terrestrial gross primary production and net primary production monitoring, Global Change Biol., 11, 666-684, 2005.

Turner, D. P., Ritts, W. D., and Cohen, W. B.: Evaluation of MODIS NPP and GPP products across multiple biomes, Remote Sens. Environ., 102, 282-293, 2006.

United Nations: Sahel Regional Strategy Mid-Year Review 2013 New York, 1-59, 2013.

Veenendaal, E. M., Kolle, O., and Lloyd, J.: Seasonal variation in energy fluxes and carbon dioxide exchange for a broadleaved semi-arid savanna (Mopane woodland) in Southern Africa, Global Change Biol., 10, 318-328, 2004.

Velluet, C., Demarty, J., Cappelaere, B., Braud, I., Issoufou, H. B. A., Boulain, N., Ramier, D., Mainassara, I., Charvet, G., Boucher, M., Chazarin, J. P., Oï, M., Yahou, H., Maidaji, B., Arpin-Pont, F., Benarrosh, N., Mahamane, A., Nazoumou, Y., Favreau, G., and Seghieri, J.: Building a field- and model-based climatology of local water and energy cycles in the cultivated Sahel; annual budgets and seasonality, Hydrol. Earth Syst. Sci., 18, 5001-5024, 10.5194/hess-18-5001-2014, 2014.

Yoder, B. J., and Pettigrew-Crosby, R. E.: Predicting nitrogen and chlorophyll content and concentrations from reflectance spectra (400–2500 nm) at leaf and canopy scales, Remote Sens. Environ., 53, 199-211, http://dx.doi.org/10.1016/0034-4257(95)00135-N, 1995.

Zhang, Y., Guanter, L., Berry, J. A., Joiner, J., van der Tol, C., Huete, A., Gitelson, A., Voigt, M., and Köhler, P.: Estimation of vegetation photosynthetic capacity from space-based measurements of chlorophyll fluorescence for terrestrial biosphere models, Global Change Biol., 20, 3727-3742, 10.1111/gcb.12664, 2014.

Tables

Table 1. Description of the six measurement sites including location, soil type, ecosystem type and dominant species.

Measurement site	Coordinates	Soil type	Ecosystem	Dominant species
Agoufou[a] (ML-AgG, Mali)	15.34°N, 1.48°W	Sandy ferruginous Arenosol	Open woody savannah (4% tree cover)	Trees: *Acacia spp.*, *Balanites aegyptiaca, Combretum glutinosum* *Herbs: Zornia glochidiata, Cenchrus biflorus, Aristida mutabilis*, *Tragus berteronianus*
Dahra[b] (SN-Dah, Senegal)	15.40°N, 15.43°W	Sandy luvic arenosol	Grassland/shrubland Savanna (3% tree cover)	Trees: *Acacia spp.*, *Balanites aegyptiaca* Herbs: *Zornia latifolia*, *Aristida adscensionis*, *Cenchrus biflorus*
Demokeya[c] (SD-Dem, Sudan)	13.28°N, 30.48°E	Cambic Arenosol	Sparse acacia savannah (7% tree cover)	*Trees: Acacia spp.,* Herbs: *Aristida pallida, Eragrostis tremula*, *Cenchrus biflorus*
Kelma[a] (ML-Kem, Mali)	15.22°N, 1.57°W	Clay soil depression	Open acacia forest (90% tree cover)	Trees: *Acacia seyal*, *Acacia nilotica*, *Balanites aegyptiaca* Herbs: *Sporobolus hevolvus, Echinochloa colona, Aeschinomene sensitive*
Wankama Fallow[d] (NE-WaF, Niger)	13.65°N, 2.63°E	Sandy ferruginous Arenosol	Fallow bush	*Guiera senegalensis*
Wankama Millet[e] (NE-WaM, Niger)	13.64°N, 2.63°E	Sandy ferruginous Arenosol	Millet crop	*Pennisetum glaucum*

[a](Timouk et al., 2009)
[b](Tagesson et al., 2015b)
[c](Sjöström et al., 2009)
[d](Velluet et al., 2014)
[e](Boulain et al., 2009)

Table 2. Correlation between intra-annual dynamics in photosynthetic capacity (F_{opt}; F_{opt_frac} for all sites), quantum efficiency (α; $\alpha_{\_frac}$ for all sites), and the different vegetation indices for the six measurement sites (Fig. 1). Values are averages±1 standard deviation from 200 bootstraping runs. The bold values are the indices with the strongest correlation. EVI is the enhanced vegetation index, NDVI is the normalized difference vegetation index, RDVI is the renormalized difference vegetation index, SIWSI is the shortwave infrared water stress index. $SIWSI_{12}$ is based on the MODIS Bidirectional Reflectance Distribution Functions (NBAR) band 2 and band 5, whereas $SIWSI_{16}$ is based on MODIS NBAR band 2 and band 6.

Measurement site	F_{opt}					α				
	EVI	NDVI	RDVI	$SIWSI_{12}$	$SIWSI_{16}$	EVI	NDVI	RDVI	$SIWSI_{12}$	$SIWSI_{16}$
ML-AgG	0.89±0.02	0.87±0.02	0.95±0.01	**-0.95±0.01**	-0.93±0.02	0.92±0.02	0.91±0.01	**0.96±0.01**	-0.94±0.01	-0.88±0.02
SN-Dah	0.92±0.005	0.91±0.01	0.96±0.003	**-0.96±0.004**	-0.93±0.01	0.89±0.01	0.90±0.01	**0.93±0.01**	-0.92±0.01	-0.87±0.01
SD-Dem	0.81±0.01	0.78±0.01	0.91±0.01	**-0.93±0.01**	-0.90±0.01	0.76±0.02	0.73±0.02	**0.86±0.01**	-0.82±0.02	-0.79±0.02
MA-Kem	0.77±0.02	0.83±0.02	0.95±0.01	**-0.95±0.01**	-0.90±0.02	0.69±0.05	0.73±0.04	**0.80±0.03**	-0.77±0.03	-0.76±0.03
NE-WaF	0.87±0.02	0.81±0.02	0.78±0.02	**-0.90±0.01**	-0.80±0.02	**0.89±0.01**	0.84±0.01	0.85±0.01	-0.88±0.01	-0.79±0.01
NE-WaM	0.41±0.05	0.50±0.04	**0.72±0.03**	-0.55±0.04	-0.43±0.05	0.72±0.02	0.76±0.02	**0.81±0.01**	-0.75±0.01	-0.72±0.01
All sites	0.86±0.0	0.79±0.0	**0.90±0.0**	0.75±0.0	0.70±0.0	0.83±0.01	0.80±0.01	**0.86±0.01**	0.62±0.01	0.54±0.01

Table 3. Statistics for the regression tree analysis. The regression tree analysis was used for studying relationships between intra-annual dynamics in the the photosynthetic capacity (F_{opt}; F_{opt_frac} for all sites) and quantum efficiency (α; $α_{\_frac}$ for all sites) and the explanatory variables for the six measurement sites (Fig. 1). The pruning level is the number of splits of the regression tree and an indication of complexity of the system.

Measurement site	Explanatory variables:					Pruning level	R^2
F_{opt}	1	2	3	4	5		
ML-AgG	$SIWSI_{12}$	Tair	PAR	SWC		16	0.98
SN-Dah	$SIWSI_{12}$	SWC	VPD	Tair	PAR	84	0.98
SD-Dem	$SIWSI_{12}$	VPD	SWC	Tair	PAR	33	0.97
ML-Kem	$SIWSI_{12}$	PAR	Tair	VPD		22	0.98
NE-WaF	$SIWSI_{12}$	SWC	VPD	Tair		14	0.92
NE-WaM	RDVI	SWC	VPD	Tair		18	0.75
All sites	RDVI	SWC	Tair	VPD		16	0.87
α							
ML-AgG	RDVI					3	0.95
SN-Dah	RDVI	VPD	SWC	Tair	PAR	21	0.93
SD-Dem	RDVI	SWC	PAR	Tair		16	0.93
ML-Kem	RDVI	Tair				4	0.75
NE-WaF	EVI	SWC	VPD			10	0.90
NE-WaM	RDVI	SWC	VPD	Tair		15	0.86
All sites	RDVI	SWC	VPD	Tair		16	0.84

Table 4. Annual peak values of quantum efficiency (α_{peak}; μmol CO_2 μmol PAR^{-1}) and photosynthetic capacity (F_{opt_peak}; μmol CO_2 m^{-2} s^{-1}) for the six measurement sites (Fig. 1). The peak values are the 2 week running mean with highest annual value.

Measurement site	Year	α_{peak}	F_{opt_peak}
ML-AgG	2007	0.0396	24.5
SN-Dah	2010	0.0638	50.0
	2011	0.0507	42.3
	2012	0.0480	39.2
	2013	0.0549	40.0
SD-Dem	2007	0.0257	16.5
	2008	0.0327	21.0
	2009	0.0368	16.5
ML-Kem	2007	0.0526	33.5
NE-WaF	2005	0.0273	18.2
	2006	0.0413	21.0
NE-WaM	2005	0.0252	10.6
	2006	0.0200	10.1
Average		0.0399	26.4

Table 5. Correlation matrix between annual peak values of photosynthetic capacity (F_{opt_peak}) and quantum efficiency (α_{peak}) and measured environmental variables. P is annual rainfall; T_{air} is yearly averaged air temperature at 2 m height; SWC is yearly averaged soil water content (% volumetric water content) measured at 0.1 m depth; Rh is yearly averaged relative humidity; VPD is yearly averaged vapour pressure deficit; R_g is yearly averaged incoming global radiation; N and C cont. are soil nitrogen and carbon contents; $NDVI_{peak}$ is annual peak normalized difference vegetation index (NDVI); EVI_{peak} is annual peak enhanced vegetation index (EVI); $RDVI_{peak}$ is annual peak renormalized difference vegetation index (RDVI); $SIWSI_{12peak}$ is annual peak short wave infrared water stress index based on MODIS NBAR band 2 and band 5; and $SIWSI_{16peak}$ is annual peak short wave infrared water stress index based on MODIS NBAR band 2 and band 6. Sample size was 13 for all except the marked explanatory variables.

Explanatory variable	F_{opt_peak}	α_{peak}
Meteorological data		
P (mm)	0.24±0.26	0.13±0.27
T_{air} (°C)	-0.07±0.25	-0.01±0.25
SWC (%)[a]	0.33±0.25	0.16±0.27
Rh (%)	0.73±0.16*	0.60±0.19
VPD (hPa)	0.20±0.26	0.15±0.30
R_g (W m^{-2})	-0.48±0.21	-0.41±0.24
Biomass and edaphic data		
Biomass (g DW m^{-2})[a]	0.77±0.15*	0.74±0.14*
C3/C4 ratio	-0.05±0.26	0.06±0.30
N cont. (%)[b]	0.22±0.11	0.35±0.14
C cont. (%)[b]	0.89±0.06**	0.87±0.07**
Earth observation data		
$NDVI_{peak}$	0.94±0.05**	0.87±0.07**
EVI_{peak}	0.93±0.04**	0.87±0.07**
$RDVI_{peak}$	0.93±0.04**	0.89±0.07**
$SIWSI_{12peak}$	0.85±0.08**	0.84±0.08**
$SIWSI_{16peak}$	0.67±0.12*	0.65±0.15*
Photosynthetic variables		
F_{opt}	-	0.94±0.03**

[a]sample size equals 11.
[b]sample size equals 9.
* significant at 0.05 level.
** significant at 0.01 level

Table 6. Statistics regarding the evaluation of the gross primary production (GPP) model for the six measurement sites (Fig. 1). In situ and modelled GPP are averages ± 1 standard deviation. RMSE is the root-mean-squares-error, and slope, intercept and R^2 is from the fitted ordinary least squares linear regression.

Measurement site	In situ GPP (µmol CO_2 m^{-2} s^{-1})	Modelled GPP (µmol CO_2 m^{-2} s^{-1})	RMSE (µmol CO_2 m^{-2} s^{-1})	slope	Intercept (µmol CO_2 m^{-2} s^{-1})	R^2
ML-AgG	5.35±6.38	5.97±5.80	2.48±0.10	0.84±0.003	1.46±0.01	0.86±0.002
SN-Dah	9.39±10.17	8.87±9.67	3.99±1.34	0.88±0.002	0.62±0.01	0.85±0.001
SD-Dem	4.26±4.55	3.98±3.90	3.15±1.06	0.63±0.003	1.31±0.007	0.54±0.02
ML-Kem	11.16±8.02	10.52±9.22	4.35±1.23	1.02±0.003	-0.82±0.03	0.78±0.002
NE-WaF	5.77±4.17	6.63±3.53	2.47±1.05	0.70±0.005	2.58±0.02	0.69±0.003
NE-WaM	3.04±1.93	6.35±3.47	4.12±0.99	1.31±0.004	2.37±0.02	0.53±0.003
Average	6.73±7.72	7.02±7.39	3.68±0.55	0.83±0.07	1.34±0.82	0.84±0.07

Table 7. The parameters for Eq. 13 that was used in the final gross primary production (GPP) model. RMSE is the root mean square error, and R^2 is the coefficient of determination for the regression models predicting the different variables.

Parameter	Value	RMSE	R^2
k_{Fopt}	79.6±6.3	5.1±1.3	0.89±0.05
m_{Fopt}	-7.3±3.2		
l_{Fopt}	3.51±0.19	0.15±0.02	0.88±0.06
n_{Fopt}	0.03±0.006		
$_{\alpha}$	0.16±0.02	0.0069±0.0021	0.81±0.10
m_{α}	-0.014±0.007		
l_{α}	3.75±0.27	0.20±0.02	0.80±0.10
n_{α}	0.02±0.007		

Figures

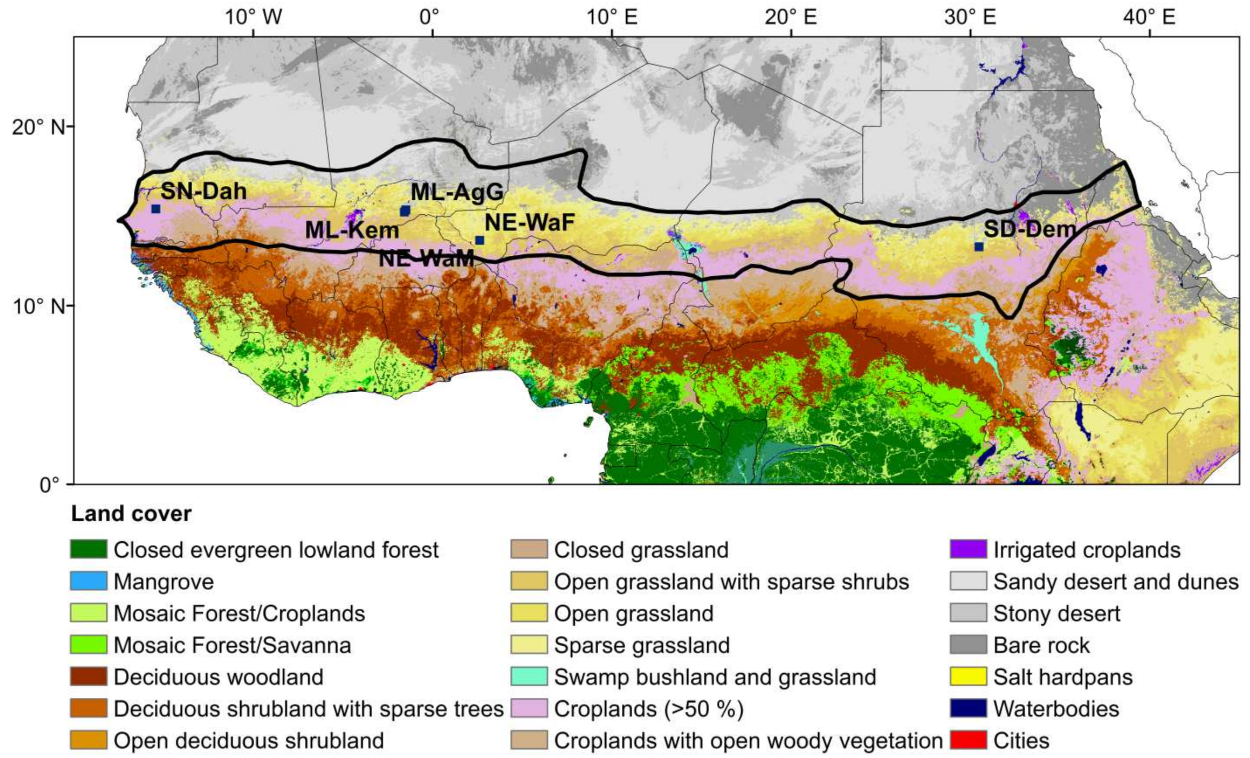

Figure 1. Land cover classes for the Sahel and the location of the six measurement sites included in the study. The land cover classes are based on multi-sensor satellite observations (Mayaux et al., 2003). The sites are Agoufou (ML-AgG), Dahra (SN-Dah), Demokeya (SD-Dem), Kelma (ML-Kem), Wankama Fallow (NE-WaF), and Wankama Millet (NE-WaM). The thick black line is the borders of the Sahel based on the isohytes 150 and 700 mm of annual precipitation (Prince et al., 1995).

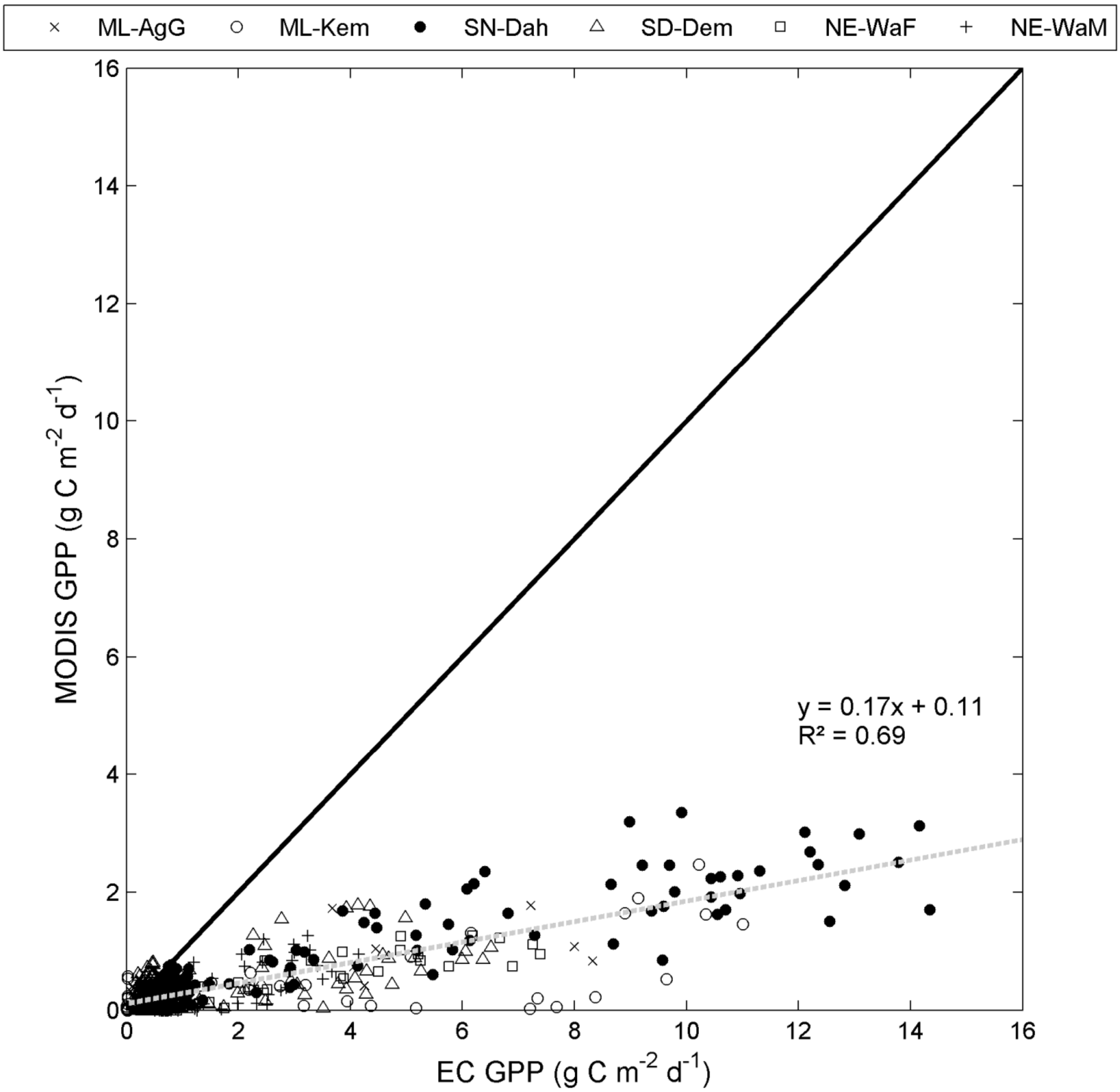

Figure 2. Evaluation of the MODIS based GPP product MOD17A2H collection 6 against eddy covariance based GPP from the six measurement sites (Fig. 1) across the Sahel. The thick black line shows the one-to-one ratio, and the grey dotted line is the fitted ordinary least square linear regression.

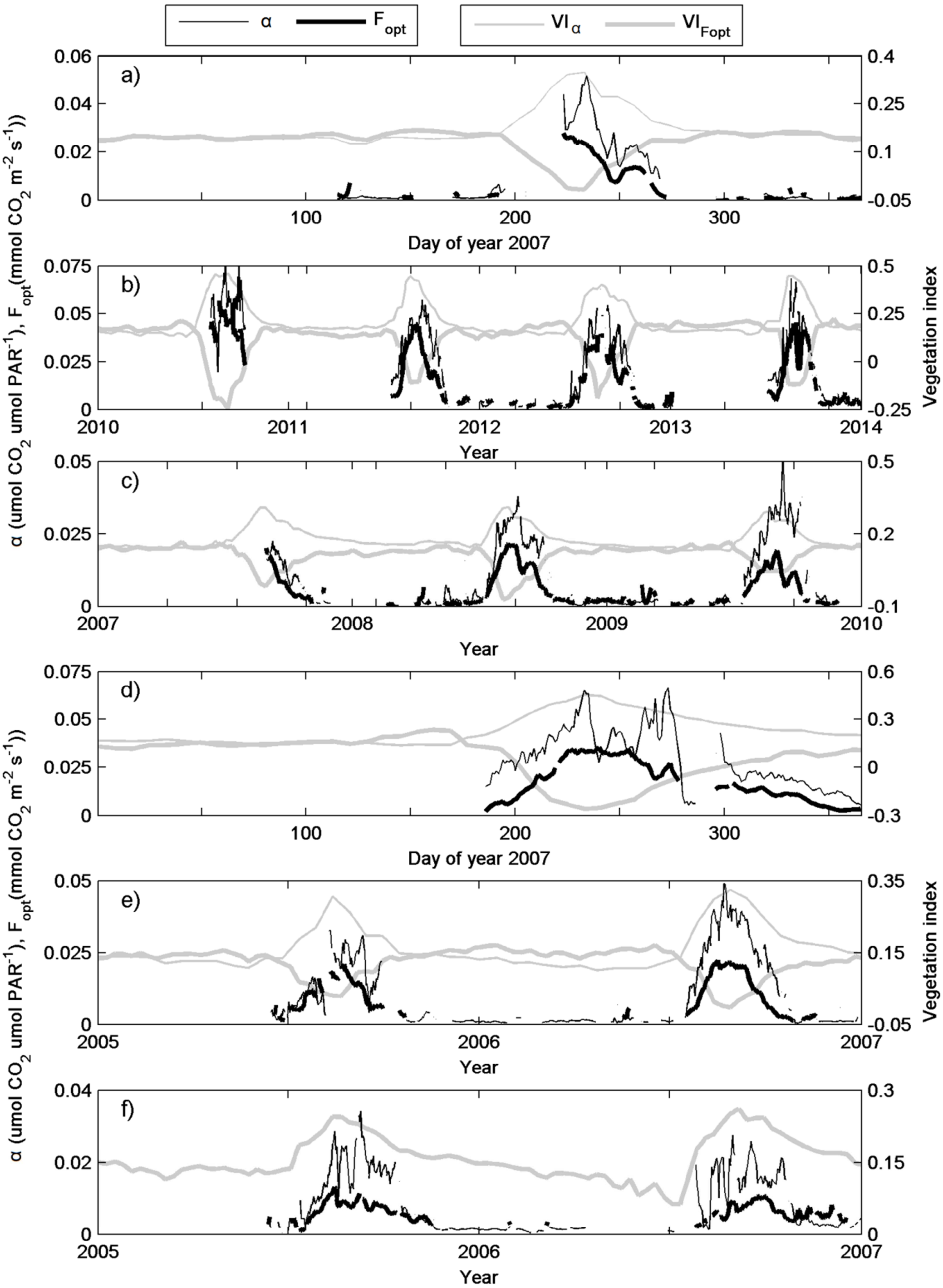

α
F_{opt}
VI_{α}
VI_{Fopt}
a)
b)
c)
d)
e)
f)
Day of year 2007
Year
α (umol CO_2 umol PAR^{-1}), F_{opt}(mmol CO_2 m^{-2} s^{-1}))
Vegetation index

Figure 3. Dynamics in photosynthetic capacity (F_{opt}) and quantum efficiency (α) for the six measurement sites. Included is also dynamics in the vegetation indices with highest correlation to the intra-annual dynamics in F_{opt} (VI_{Fopt}) and to quantum efficiency (VI_{α}) (Table 2). The sites are a) Agoufou (ML-AgG), b) Dahra (SN-Dah), c) Demokeya (SD-Dem), d) Kelma (ML-Kem), e) Wankama Fallow (NE-WaF), and f) Wankama Millet (NE-WaM).

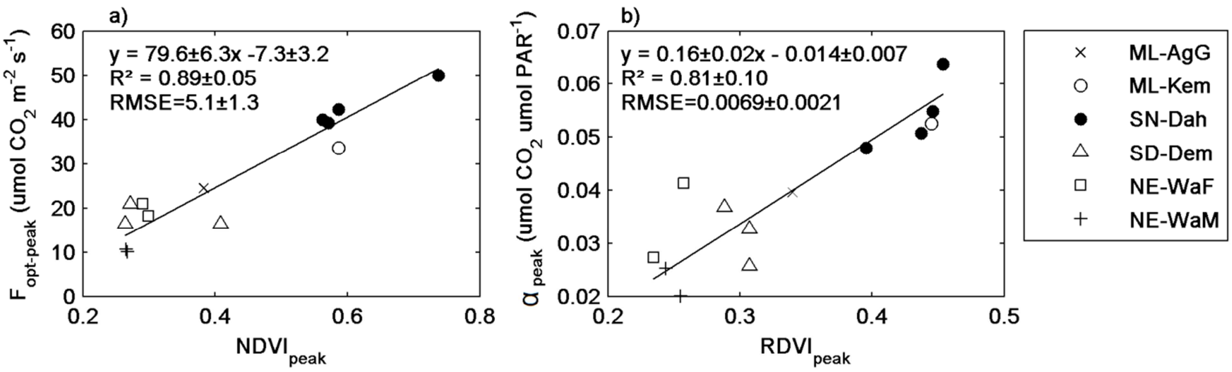

Figure 4. Scatter plots of annual peak values for the six measurement sites (Fig. 1) of a) photosynthetic capacity (F_{opt_peak}) and b) quantum efficiency (α_{peak}) against peak values of normalized difference vegetation index ($NDVI_{peak}$) and renormalized difference vegetation index ($RDVI_{peak}$), respectively. The annual peak values were estimated by taking the annual maximum of a two week running mean.

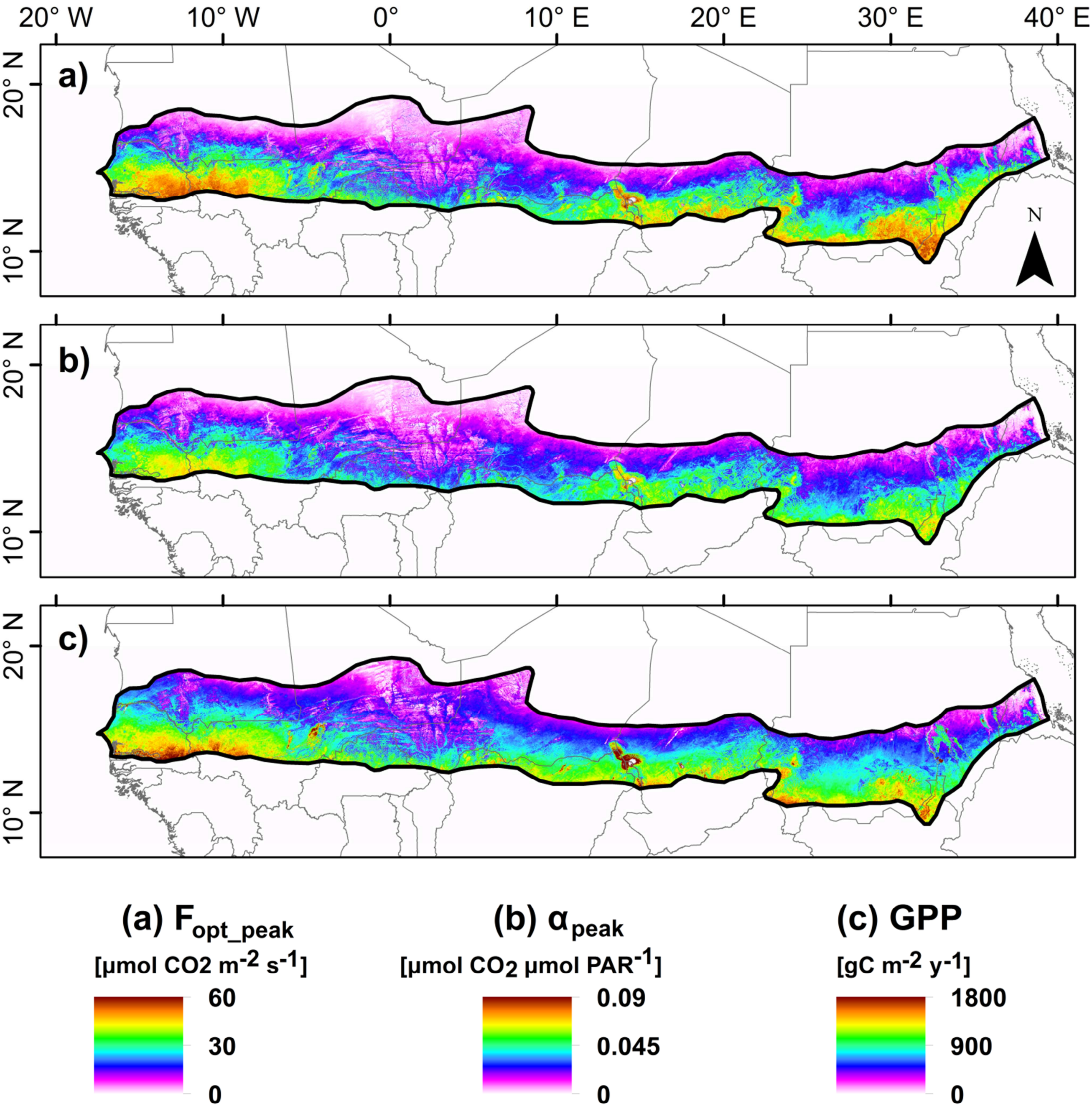

Figure 5. Maps of a) peak values of photosynthetic capacity (F_{opt_peak}) averaged for 2001-2014, b) peak values of quantum efficiency (α_{peak}) averaged for 2001-2014, and c) annual budgets of GPP averaged for 2001-2014.

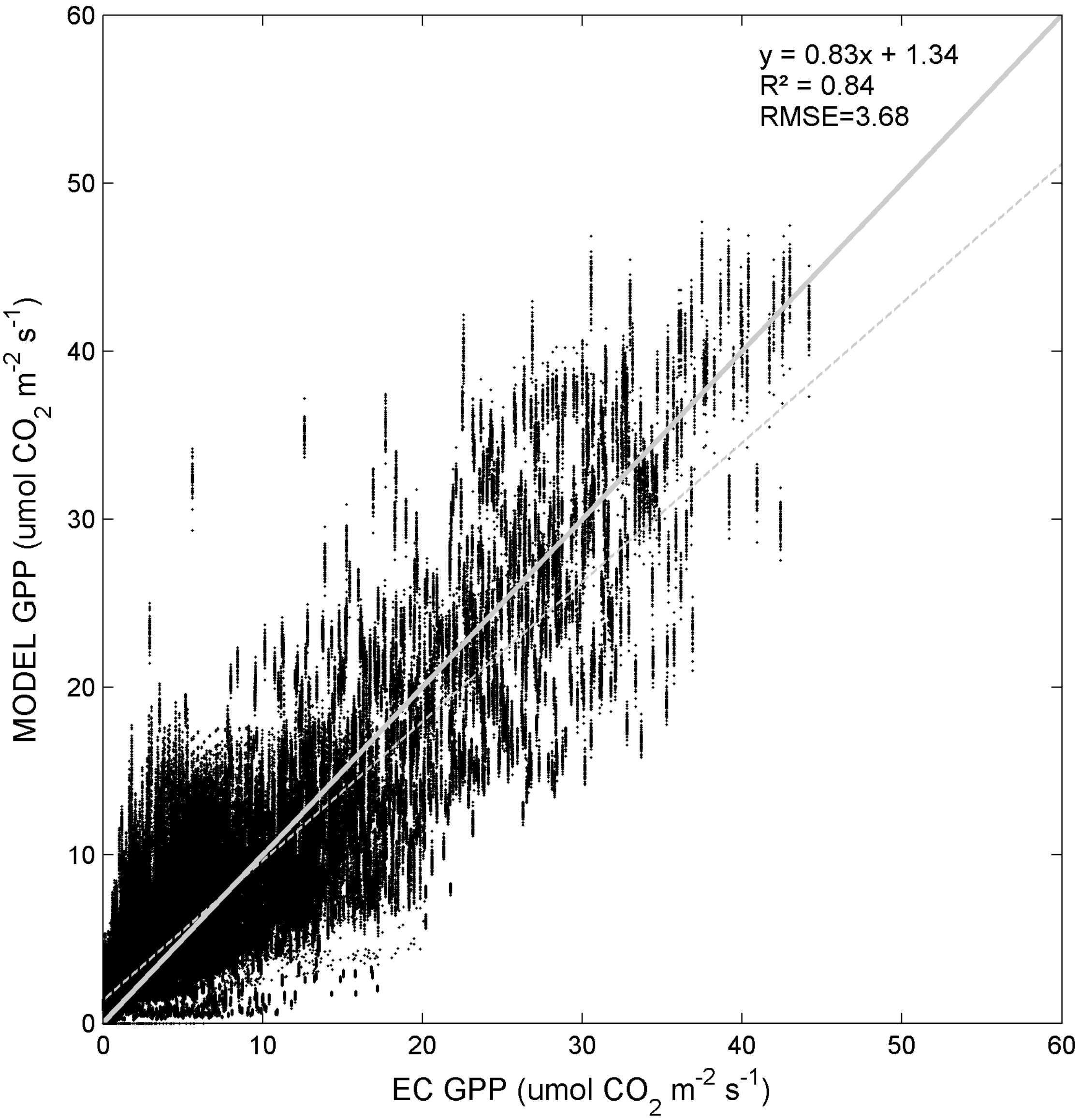

Figure 6. Evaluation of the modelled gross primary production (GPP) (Eq. 13) against in situ GPP from all six measurement sites across the Sahel. The thick grey line shows the one-to-one ratio, whereas the dotted thin grey line is the fitted ordinary least square linear regression.

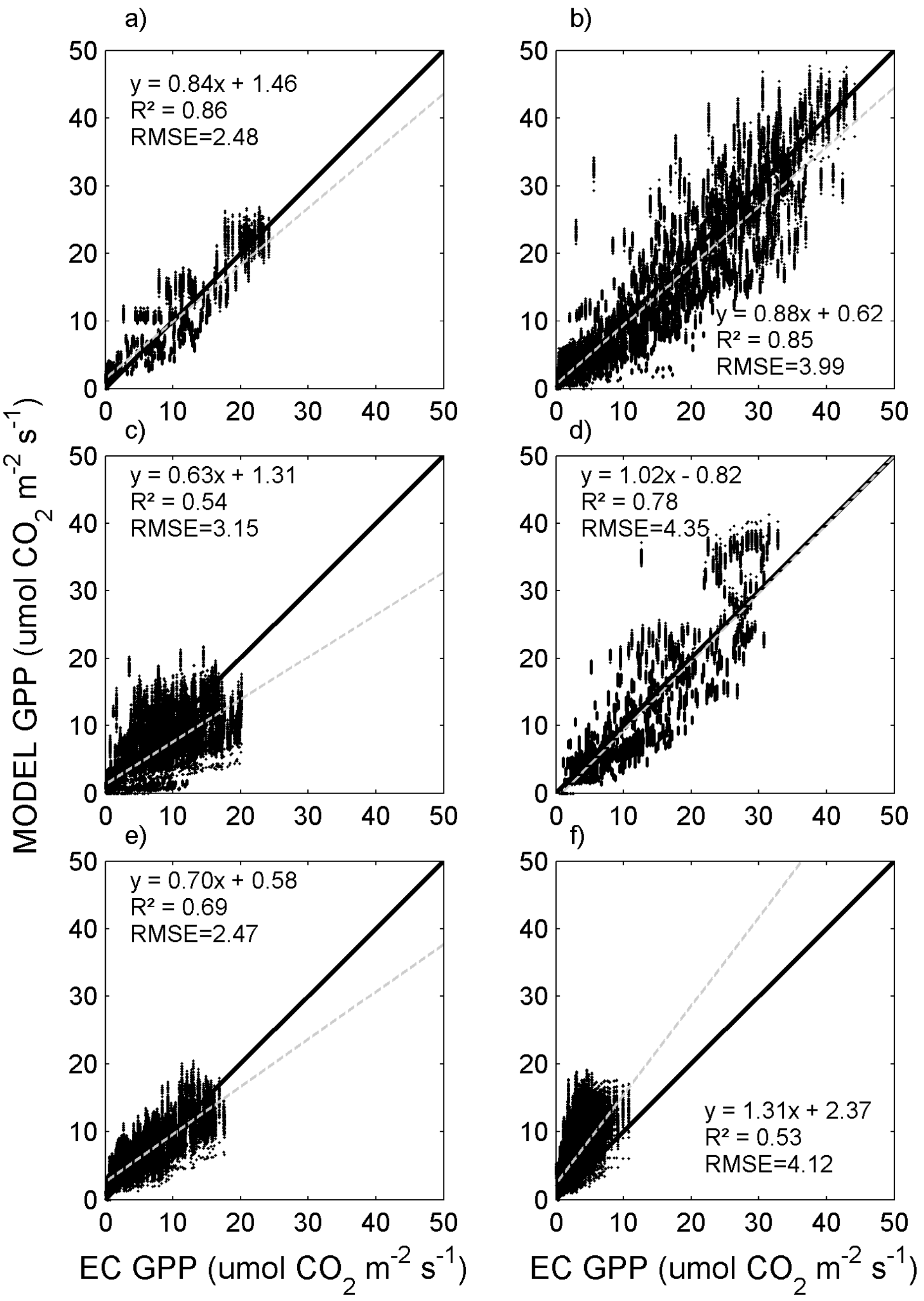

Figure 7. Evaluation of the modelled gross primary production (GPP) (Eq. 13) against in situ GPP for the six sites across Sahel (Fig. 1). The thick black line shows the one-to-one ratio, whereas the dotted thin grey line is the fitted ordinary least

square linear regression. The sites are a) Agoufou (ML-AgG), b) Dahra (SN-Dah), c) Demokeya (SD-Dem), d) Kelma (ML-Kem), e) Wankama Fallow (NE-WaF), and f) Wankama Millet (NE-WaM).